The architecture of lipid droplets in the diatom Phaeodactylum tricornutum

Josselin Lupette, Antoine Jaussaud, Khawla Seddiki, Christian Morabito, Sabine Brugière, Hubert Schaller, Marcel Kuntz, Jean-Luc Putaux, Pierre-Henri Jouneau, Fabrice Rébeillé, et al.

Title:

The architecture of lipid droplets in the diatom *Phaeodactylum tricornutum*

Authors:

Josselin Lupette[1], Antoine Jaussaud[1], Khawla Seddiki[1,§], Christian Morabito[1], Sabine Brugière[2], Hubert Schaller[3], Marcel Kuntz[1], Jean-Luc Putaux[4], Pierre-Henri Jouneau[5], Fabrice Rébeillé[1], Denis Falconet[1], Yohann Couté[2], Juliette Jouhet[1], Marianne Tardif[2], Juliette Salvaing[1], Eric Maréchal[1,*]

Affiliations:

[1] Laboratoire de Physiologie Cellulaire et Végétale, CNRS, CEA, INRA, Université Grenoble Alpes, Institut de Biosciences et Biotechnologies de Grenoble, CEA Grenoble, 17 avenue des Martyrs, 38000, Grenoble, France.

[2] Laboratoire de Biologie à Grandes Echelles, Université Grenoble Alpes, CEA, Inserm, Institut de Biosciences Biotechnologies de Grenoble, CEA Grenoble, 17 avenue des Martyrs, 38000, Grenoble, France.

[3] Institut de Biologie Moléculaire des Plantes, CNRS, 12 Rue du général Zimmer, 67084, Strasbourg Cedex, France.

[4] Centre de Recherches sur les Macromolécules Végétales (CERMAV), CNRS, Université Grenoble Alpes, 38000, Grenoble, France.

[5] Laboratoire d'Etudes des Matériaux par Microscopie Avancée; Institut Nanosciences et Cryogénie; Service de Physique des matériaux et Microstructures; CEA-Grenoble; 17 rue des Martyrs; 38000 Grenoble, France

[*] Correspondence: eric.marechal@cea.fr

[§] Present address: Proteomics Platform Center, Centre de recherche du CHU de Quebec, Faculty of Medicine, Universite Laval, Quebec City, Quebec, Canada.

Abstract

Diatoms are a major phylum of phytoplankton biodiversity and a resource considered for biotechnological developments, as feedstock for biofuels and applications ranging from food, human health or green chemistry. They contain a secondary plastid limited by four membranes, the outermost one being connected with the endoplasmic reticulum (ER). Upon nitrogen stress, diatoms reallocate carbon to triacylglycerol storage inside lipid droplets (LDs). The comprehensive glycerolipid and sterol composition and the architecture of diatom LDs are unknown. In *Phaeodactylum tricornutum*, LDs are in contact with plastid, mitochondria and uncharacterized endomembranes. We purified LDs from nitrogen-starved *P. tricornutum* cells to high purity level (99 mol% triacylglycerol of total glycerolipids). We used the Stramenopile Lipid Droplet Protein (StLDP) as a previoulsy validated marker for the identity of *P. tricornutum* LD. Amphipathic lipids surrounding LDs consist of a betaine lipid, diacylglycerylhydroxymethyltrimethyl-β-alanine (0.4 mol%); sulfoquinovosyldiacylglycerol (0.35 mol%); phosphatidylcholine (0.15 mol%) and one sterol, brassicasterol. By contrast with whole cell extracts, the betaine lipid from LDs only contains eicosapentaenoic acid paired with palmitoleic or palmitolenic acids. This polar lipid composition suggests a budding of LDs from the cytosolic leaflet of the plastid outermost membrane. LD pigments reveal a specific accumulation of *β*-carotene. The LD proteome obtained from three independent biological replicates, based on stringent filtering of extracted data, and following subtraction of proteins downregulated by nitrogen starvation, highlights a core proteome of 86 proteins, including StLDP. LD-associated proteins suggest connections with vesicular trafficking (coatomer, clathrin), cytoskeleton, plastid and mitochondria. Unsuspected LD-associated function include protein synthesis (ribosomes), folding (chaperones), posttranslational modifications and quality control (ubiquitination and ERAD pathway), possibly preparing translation of specific mRNAs. The detection of histone proteins, as previously demonstrated in drosophila embryo LDs, also suggests the storage of nucleosome components, preparing cell division and chromatin packaging, when cells are not stressed anymore.

Keywords

Diatoms, *Phaeodactylum*, secondary plastid, lipid droplets, triacylglycerol, betaine lipid, carotenoids, histones.

1. Introduction

The biodiversity of phytoplankton is immense [1], ranging from cyanobacteria to photosynthetic eukaryotes that contain either a chloroplast inherited from a primary endosymbiosis, like in green algae, [2-4] or a complex photosynthetic organelle inherited from a secondary endosymbiosis, like in heterokonts [5-7]. Diatoms represent one of the largest groups of heterokonts, dominating oceanic and fresh water ecosystems, and contributing significantly to biogeochemical cycles, both as primary producers at the basis of food webs and as carriers of carbon and silicon towards the ocean interior [8]. Diatoms have also attracted the attention as a promising resource for biotechnological developments, as feedstock for biofuels and applications ranging from food, human health or green chemistry [9-12]. In spite of their importance in eukaryote's evolution, role in ecosystems and potential for biotechnologies, knowledge of diatom subcellular architecture and physiology is still poor. Efforts need to be pursued, in such models as *Phaeodactylum tricornutum* [13-15].

Diatoms living in oceans and fresh waters are permanently exposed to environmental variations and stresses. Nutrient starvation [14, 16, 17], high temperature [18, 19], high light [19], exposure to nitric oxide [20], to hydrogen peroxide [21-23] or to a variety of chemicals [24-27] are known to trigger an intense lipid remodeling marked by an accumulation of lipid droplets (LDs) within cells. The rational for LD formation as part of general stress responses is not fully comprehended.

LDs are ubiquitously found in prokaryotic and eukaryotic cells [28-30]. Their architecture is based on a hydrophobic core containing neutral lipids, such as triacylglycerols (TAG), steryl esters, hydrophobic pigments etc. This core is surrounded by a monolayer of polar lipids, mainly phospholipids, with embedded or transiently associated proteins [28, 31]. In our current understanding and based on works achieved on yeasts or mammals, the biogenesis of LDs occurs at the outer leaflet of the endoplasmic reticulum (ER) [28, 32, 33]. The proteome of nascent and budding LDs can therefore include (1) ER-located enzymes synthesizing neutral lipids, such as diacylglycerol acyltransferases (DGATs) or phosphatidylcholine:diacylglycerol acyltransferases (PDATs), (2) proteins involved in LD overall assembly like seipins, and (3) structural proteins stabilizing its sub-spherical shape and protecting its hydrophobic core. In more mature LDs, associated proteins can include (4) enzymes involved in the hydrolysis of neutral lipids, mainly TAG lipases, and conversion of fatty acids into other metabolites, as well as (5) proteins involved in the docking to the cytoskeleton and organelles, such as mitochondria or peroxisomes, or eventually (6) proteins involved in other functions [28, 34, 35]. In each

environmental and physiological context, the function of the LD depends on its protein equipment [28, 34, 35]. The understanding of LD architecture and function requires therefore a precise inventory of its lipophilic and protein components.

LD-associated proteins are not conserved in evolution, and it is therefore necessary to determine the proteome of LDs in each major clade. Besides the differences, a structural classification of proteins has been proposed [36], with class I proteins having a hydrophobic 'hairpin' motif, such as plant oleosins, caleosin and stereoleosins [37, 38], accessing LDs from the ER either during LD formation (budding) or after LD maturation via ER–LD membrane bridges. Class II proteins, such as mammal's perilipins [36, 39], access the LD surface from the cytosol, binding to LDs through amphipathic helices or other hydrophobic domains. Additional proteins can also bind to LD following protein–protein interactions [36].

Proteomic analyses of nitrogen stress-induced LDs have been conducted in cells of Chlorophyta (green algae) containing a primary plastid, like *Chlamydomonas reinhardtii* [16, 40, 41], *Chlorella sp.* [42], *Haematococcus pluvialis* [43], three *Dunaliella* species [44], *Scenedesmus quadricauda* [45], or *Lobosphaera incisa* [46]. All these studies have highlighted the presence of major structural proteins. In some green algae like *Chlamydomonas*, an important set of enzymes involved in TAG formation was still associated to the mature LDs, as well as components of a multimeric ABC transporter of the chloroplast envelope involved in lipid transfers, suggesting a role of this organelle in providing precursors for some of the TAGs accumulating in LDs [16].

In diatoms, by contrast, the secondary plastid is delineated by four membranes and the outermost one is continuous with the nuclear envelope and therefore connected to the endomembrane system, including the ER [47] (Fig. 1). The outermost membrane of the plastid, or epiplastid membrane (EpM) [7] is therefore likely to share some functions with the ER. The electron microscopy images of cells of the pennate diatom *P. tricornutum* shows tight connections between the LD and the EpM (LD-EpM contact sites), endomembrane vesicles (LD-endomembrane contact sites) and the mitochondria outer envelope membrane (LD-mitochondria contact sites) [47] (Fig. 1). It is not known whether the LD-EpM contact corresponds to a site of LD biogenesis, following the proposed model of LD-budding from the ER in mammal and yeast cells, or if it corresponds to independent functional interactions. Based on electron microscopy, it is not yet possible to determine whether endomembrane vesicles interacting with the LD correspond to the ER, peroxisomes or other compartments. LD-mitochondria contact sites are also observed [47] (Fig. 1), consistently with a docking to an

organelle, where beta-oxidation of FAs could occur. The proteome of diatom LDs could possibly comprise proteins involved in these inter-organellar interactions.

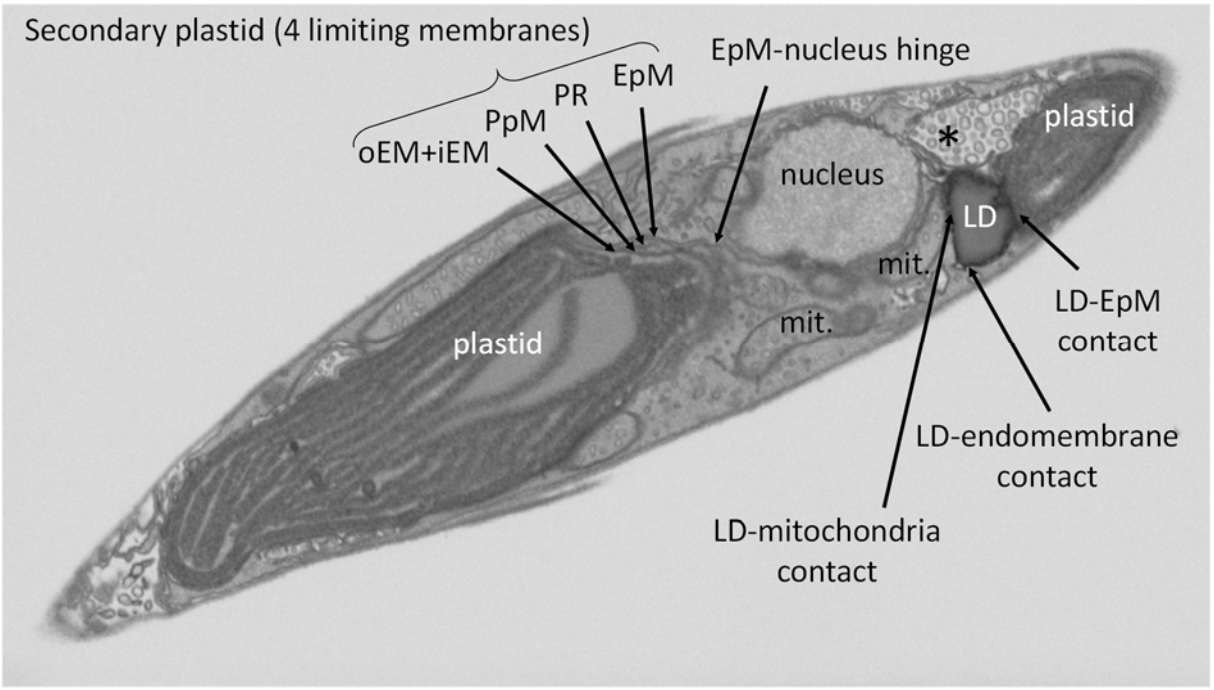

Figure 1: Interactions of the lipid droplet of *P. tricornutum* with other organelles. Cells were collected in late exponential phase (beginning of nitrogen starvation). iEM, chloroplast inner envelope membrane; LD, lipid droplet; mit, mitochondria; PR, periplastid reticulum; PPM, periplastid membrane; oEM, chloroplast outer envelope membrane; EpM, epiplastid membrane; *, an uncharacterized endomembrane compartment differing from the mitochondrion by the absence of an electron-dense matrix and the presence of vesicles inside a membrane sack.

Recent proteomic studies of nitrogen stress induced LDs in photosynthetic heterokonts have been performed in the pennate diatoms *Fistulifera solaris* [48] and *P. tricornutum* [49], allowing the identification of 15 and 5 putative LD proteins respectively, as well as in the eustigmatophyte *Nannochloropsis oceanica* [50]. These studies have mostly focused on the search for major structural proteins covering the surface of the LDs and ensuring its stability and controlling its size.

Here we addressed the architecture of the mature LD induced by nitrogen starvation, inside the cells of *P. tricornutum*. In LD-enriched fractions purified on a sucrose density gradient, five proteins have been previously described, *i.e.* a major Stramenopile LD Protein (StLDP - Phatr3_J48859), an Acyl-CoA-binding protein (Phatr3_J48778), a heat shock protein (HSP70 - Phatr3_J54019) and two hypothetical proteins possibly involved in redox reactions (Phatr3_J45894 and Phatr3_J49981) [49]. The StLDP is a class I protein of 456 amino acids (49 kDa) having a hydrophobic domain of 54 amino acids (in position 222-275) forming a pattern $X_7PX_9PX_{10}PX_3PX_{23}$ (with P a proline) [49]. The expression of the *stldp* gene is upregulated upon nitrogen starvation [49].

The location of the StLDP at the LD has been confirmed based on GFP-fusion imaging [51]. The StLDP is therefore a validated marker of *Phaedactylum* LD induced by nitrogen starvation. In the present study, we refined the method to prepare highly purified LDs from *P. tricornutum* cells and performed a comprehensive analysis of the lipids, pigments and proteome, allowing the characterization of LD components and revealing unsuspected roles.

2. Materials and methods

2.1. Cultivation of Phaeodactylum tricornutum

Phaeodactylum tricornutum (Pt1) Bohlin Strain 8.6 CCMP2561 (Culture Collection of Marine Phytoplankton, now known as NCMA: National Center for Marine Algae and Microbiota) was used in all experiments. Pt1 cells were maintained and grown in a volume of 1 L in 2-L flasks at 20°C, in a modified ESAW (Enriched Seawater, Artificial Water) medium (NaCl 362.7 mM; Na_2SO_4 25 mM; KCl 8.03 mM; $NaHCO_3$ 2.067 mM; KBr 0.725 mM; H_3BO_3 0.372 mM; NaF 0.0657 mM; $MgCl_2$ 47.18 mM; $CaCl_2$ 9.134 mM; $SrCl_2$ 0.082 mM; Na_2-glycerophosphate 21.8 µM; Na_2SiO_3 105.6 µM; disodium ethylenediaminetetraacetate dehydrate (Na_2EDTA) 14.86 µM; $Fe(NH_4)_2(SO_4)_2$ 5.97 µM; $FeCl_3$ 0.592 µM; $MnSO_4$ 2.42 µM; $ZnSO_4$ 0.254 µM; $CoSO_4$ 0.0569 µM; Na_2MoO_4 0.52 µM; H_3BO_3 61.46 µM; Na_2SeO_3 10 nM; biotin (vitamin H) 8.18 nM; cobalamin (vitamin B_{12}) 2.94 nM; thiamine (vitamin B_1) 0.594 µM) [52] using ten times enriched nitrogen and phosphate sources (10N10P containing 5.49 mM $NaNO_3$ and 0.224 mM NaH_3PO_4) [14]. Nitrogen starvation was performed by transferring cells to the same medium without any addition of $NaNO_3$ (00N10P medium). Cells were grown on a 12:12 light (50 µE $m^{-2}.sec^{-1}$) / dark cycle. Growth was evaluated by cell counting using a TECAN infinite M1000Pro plate reader and determined following the equation $y=1.834.10^{-08}\,x + 0.03758$ with x= the absorbance at 730 nm and y= the number of cells [24].

2.2. Evaluation of neutral lipid accumulation by Nile Red staining

Accumulation of triacylglycerol droplets was monitored by Nile Red (Sigma Aldrich) fluorescent staining as previously described [14, 53]. In brief, cells were diluted and adjusted to a cell density that was linearly correlated with Nile Red fluorescence. Nile Red solution (40 µL of a 2.5 $\mu g.mL^{-1}$ stock solution in DMSO) was added to 160 µL cell suspensions. LD stained with Nile Red were then visualized using a using a Zeiss LSM800 confocal laser scanning microscope equipped with a Zeiss Plan-APO x63-numerical aperture 1.46 oil immersion objective and enlarged x4. Nile Red fluorescence was monitored by excitation at 488 nm and capture zone ranging from 579 nm to 641 nm. Chlorophyll fluorescence was monitored by excitation at 488 nm and by capture zone ranging from 650 nm to 700 nm. Bright field acquisitions were also performed. Acquisition were saved under the Zeiss .czi format and imported with ImageJ 1.48v thanks to the BIO-FORMATS plugins 5.7.2. Alternatively, Nile red fluorescence values were normalized to the cell concentration.

2.3. Purification of lipid droplets

Lipid droplet (LD) purification was carried out in three independent biological replicates, from *P. tricornutum* cells cultivated in a 3-L volume (10N10P), up to a cell concentration of 5 x 10^6 cells.mL^{-1}, then subjected to nitrogen starvation (00N10P) for 7 days. Cells were collected by centrifugation at 6,000 x g, 4°C for 20 minutes (JLA 10.500 rotor, Beckman Coulter, Brea, CA, USA) and resuspended using a salt buffer (10 mM Tris-HCl + 2% NaCl). Cells were then collected by an additional centrifugation at 6,000 x g, 4°C for 20 minutes and resuspended in 50 mL of a sucrose buffer (sucrose 0.25 M; EDTA 1 mM; Tris-HCl 10 mM, final concentration, pH 7.6) supplemented with a protease inhibitor cocktail (cOmplete, Roche Diagnostics). Concentrated cells were broken using a cell disruption systems (Constant Systems Limited, Daventry, UK) set at a 2 kbar rupture pressure. Cell breakage was verified by confocal imaging. Presence of LDs was assessed by Nile red staining as described above. The broken cells were centrifuged at 48,000 x g (JA 20 Rotor, Beckman Coulter, Brea, CA, USA), 4°C for 20 minutes (SS34 rotor, Beckman Coulter, Brea, CA, USA) to eliminate the largest cell debris. The supernatant was recovered and adjusted to a concentration of sucrose 1.25 M. A cushion of 4.5 mL of this fraction was loaded at the bottom of an ultracentrifuge tube (SW32ti, Beckman Coulter, Brea, CA, USA). A second layer of 7 mL sucrose 0.7 M; Triton X-100 0.2% v/v; Tris-HCl 10 mM pH 7.6 supplemented with a protease inhibitor cocktail was added gently above the sample. A third layer of 1.5 mL sucrose 0.25 M; Tris-HCl 10 mM pH 7.6 supplemented with protease inhibitor cocktail was added gently on top of the discontinuous gradient. Gradient was ultracentrifuged at 68,000 x g, 4°C for 16 hours. LDs were carefully collected at the top of the tubes and transferred into 1.5 mL tubes. LDs were washed two times in Tris-HCl 10 mM, pH 7.6 at 20,000 x g, 4°C for 10 minutes (S55A2 Rotor, Hitachi Koki, Tokyo, Japan). A volume of 6.85 mL of purified LD is obtained per purification. The enrichment in LDs was controlled in an aliquot fraction by confocal imaging, fixed in 3% agarose in Tris-HCl 10 mM pH 7.6 in order to limit LD movements.

2.4. Sample preparation for lipidomic and proteomic analyses

Each sample corresponding to whole cells and purified LDs were divided in fractions for lipidomic, pigment and proteomic analyses, respectively. For lipidomic analyses (glycerolipids, sterols, carotenoids), hydrophobic metabolites were extracted using solvents, either from freeze-dried cells corresponding to a 50 mL aliquot fraction of the nitrogen starved culture used for LD purification or from 850 µL of purified LD fractions. Whole cell lipids were extracted using the Folch method [54, 55]. In brief, freeze-dried cells were suspended in 4 mL of boiling ethanol for 5 minutes to prevent lipid degradation, and lipids were extracted by addition of 2 mL methanol and 8 mL chloroform at room temperature. The mixture was then saturated with

argon and stirred for 1 hour at room temperature. After filtration through glass wool, cell debris were rinsed with 3 mL chloroform/methanol 2:1, v/v, and 5 mL of NaCl 1% were added to the filtrate to initiate phase separation. The chloroform phase was dried under argon before solubilizing the lipid extract in 1 mL of chloroform. LD lipids were extracted using the Bligh and Dyer method [14, 56]. Extracted lipids were dried under a flow of argon and conserved at -20°C until analyses. For proteomic analyses, proteins from purified LDs were precipitated overnight at -20°C in cold acetone. Samples were centrifuged at 20,000 x g (S55A2 Rotor, Hitachi Koki, Tokyo, Japan), 0°C for 10 minutes. The supernatant was discarded and the pellet was incubated at -20°C in cold ethyl acetate for 2 hours to eliminate residual oil. Samples were centrifuged at 20,000 x g, 0°C for 10 minutes. The supernatant was discarded and the pellet was dried under a fume hood to remove traces of ethyl acetate. Three independent purifications were performed, corresponding to biological replicates. For each independent purification, LD proteins were suspended in 100 µL of a lysis buffer (urea 7 M, thiourea 2 M, 3-((3-cholamidopropyl) dimethylammonio)-1-propanesulfonate (CHAPS) 4% w/v, Triton X-100 3% v/v and SDS 2% w/v). The quantity of purified LD proteins was evaluated on 2 µL aliquots, loaded onto a SDS PAGE and stained using the SilverQuest staining kit (Invitrogen, Carlsbad, CA, USA) in comparison with known amounts of proteins from a whole cell fraction resolved in parallel. 8 µL of purified LD proteins were used for proteomic analyses. The remaining fractions (86 µL per independent purification, pooled in 258 µL) were concentrated using Ultracel - 3K filters (Merck Millipore Ltd., Tullagreen, Carrigtwohill, Ireland), and eluted in a final volume of 48 µL, used for further SDS PAGE and Western blot analyses.

2.5. Glycerolipid profiling by liquid chromatography - tandem mass spectrometry

For each whole cell and LD lipid extracts, total glycerolipids were quantified from their fatty acids (FAs): in a 10 µL aliquot fraction a known quantity of saturated 15-carbon FA (15:0) was added and all FAs were methanolyzed into methyl esters (FAME) by a 1 hour incubation in 3 mL 2.5% H_2SO_4 in pure methanol at 100°C [57]. The reaction was stopped by addition of 3 mL water, and 3 mL hexane was added for phase separation. After 20 min of incubation, the hexane phase was transferred to a new tube. FAMEs were extracted a second time via the addition, incubation and extraction of another 3 ml hexane. The combined collected hexane fractions (6 mL) were argon-dried and FAMEs were suspended in 40 µL hexane for analysis by gas chromatography coupled with flame ionization detection (GC-FID) (Perkin Elmer), using a BPX70 (SGE) column. FAMEs were identified by comparison of their retention times with those of standards (Sigma) and quantified by the surface peak method using 15:0 for calibration.

Extraction and quantification were performed with three biological replicates. Glycerolipids were then analyzed and quantified by high-pressure liquid chromatography-tandem mass spectrometry (HPLC-MS/MS), with appropriate standard lipids [58]. In brief, lipid extracts corresponding to 25 nmol of total fatty acids were dissolved in 100 µL of chloroform/methanol [2/1, v/v] containing 125 pmol of each internal standard. Internal standards used were phosphatidylethanolamine (PE) 18:0-18:0 and diacylglycerol (DAG) 18:0-22:6 from Avanti Polar Lipid, and sulfoquinovosyldiacylglycerol (SQDG) 16:0-18:0 extracted from spinach thylakoid [59] and hydrogenated [60]. Lipids were then separated by HPLC and quantified by MS/MS. Lipid classes were separated using an Agilent 1200 HPLC system using a 150 mm x 3 mm (length x internal diameter) 5 µm diol column (Macherey-Nagel), at 40°C. The mobile phases consisted of hexane/isopropanol/water/1 M ammonium acetate, pH 5.3 [625/350/24/1, v/v] (A) and isopropanol/water/1 M ammonium acetate, pH 5.3 [850/149/1, v/v] (B). The injection volume was 20 µL. After 5 min, the percentage of B was increased linearly from 0 to 100% in 30 min and kept at 100% for 15 min. This elution sequence was followed by a return to 100% A in 5 min and an equilibration for 20 min with 100% A before the next injection, leading to a total runtime of 70 min. The flow rate of the mobile phase was 200 µL/min. The distinct glycerophospholipid classes were eluted successively as a function of the polar head group. Mass spectrometric analysis was performed on a 6460 triple quadrupole mass spectrometer (Agilent) equipped with a Jet stream electrospray ion source under following settings: drying gas heater at 260°C, drying gas flow at 13 $L.min^{-1}$, sheath gas heater at 300°C, sheath gas flow at 11 $L.min^{-1}$, nebulizer pressure at 25 psi, capillary voltage at ± 5000 V and nozzle voltage at ± 1000 V. Nitrogen was used as collision gas. The quadrupoles Q1 and Q3 were operated at widest and unit resolution respectively. Phosphatidylcholine (PC) and diacylglyceryl hydroxymethyltrimethyl-β-alanine (DGTA) analyses were carried out in positive ion mode by scanning for precursors of m/z 184 and 236 respectively at a collision energy (CE) of 34 and 52 eV. SQDG analysis was carried out in negative ion mode by scanning for precursors of m/z -225 at a CE of -56eV. Phosphatidylethanolamine (PE), phosphatidylinositol (PI), phosphatidylglycerol (PG), monogalactosyldiacylglycerol (MGDG) and digalactosyldiacylglycerol (DGDG) measurements were performed in positive ion mode by scanning for neutral losses of 141 Da, 277 Da, 189 Da, 179 Da and 341 Da at CEs of 20 eV, 12 eV, 16 eV, 8 eV and 8 eV, respectively. DAG and triacylglycerol (TAG) species were identified and quantified by multiple reaction monitoring (MRM) as singly charged ions [M+NH4]+ at a CE of 16 and 22 eV respectively. Quantification was done for each lipid species by multiple reaction monitoring (MRM) with 50 ms dwell time with the various transitions

previously recorded [14]. Mass spectra were processed using the MassHunter Workstation software (Agilent) for identification and quantification of lipids. Lipid amounts (pmol) were corrected for response differences between internal standards and endogenous lipids and by comparison with a qualified control (QC). QC extract correspond to a known *P. tricornutum* lipid extract qualified and quantified by thin-layer chromatography and gas-chromatography coupled to ion flame detection as described previously [14].

2.6. Pigment extraction and HPLC analysis

Total pigments were analyzed either from *P. tricornutum* whole cells or from purified LDs. After collection by centrifugation at 11,000 x g, 4°C, for 5 minutes, 1.5 x 10^8 cells of *P. tricornutum* were resuspended in 100 µL of cold Methanol - Tris-HCl (10 mM pH 7.4). Pigments were extracted under argon, on ice and in the dark. After centrifugation at 11,000 x g, 4°C for 5 min, the supernatant was recovered, kept in the dark at 4°C, and the pellet was further extracted 3 times with methanol 100%, *i.e.*, until the pellet became white. All supernatant fractions were pooled together and dried under argon. Pigments from LDs were collected in the lipid fraction. Pigments from total extracts and LD fractions were resuspended in 100 µL of dimethylformamide before injection on a HPLC (Varian ProStar 800, Walnut Creek, CA, USA) coupled to a diode array detector. The carotenoids were separated on a C18 reverse-phase column (250 x 4.6 mm) manufactured by Macherey-Nagel using the following method. The initial mobile phase was methanol 80% / ammonium acetate 0.5 M 20%, followed by a linear gradient to 100% of a solvent B consisting of acetonitrile 90% / water 10% during 4 min, in turn followed by a linear gradient to 80% ethyl acetate / 20% B up to 20 min, a solvent composition kept for another 5 min. Identification of carotenoids was achieved by comparing retention times and spectral properties acquired on-line with authentic standards (Fucoxanthin, *β*-carotene, lycopene).

2.7. Sterol analysis

Pure LD lipids were dissolved in 500 µL benzene and stored at -20°C. Aliquots (1/10 by volume) were used as test samples to evaluate the total ion chromatograms in gas chromatography coupled to mass spectrometry (GC-MS). Samples were treated by halves as follows, to determine both esterified and free sterols. Dried extracts were saponified in 300 µL of KOH 6% in MeOH, for 1 h at 70°C. Water (0.5 volume) was added to the mixture. The non-saponifiable compounds were extracted with three volumes of *n*-hexane. The dried residue was acetylated in toluene (100 µL) in the presence of acetic anhydride (50 µL) and pyridine (40 µL) at 70°C for 1h. Reagents were air-dried (warm air stream) then the extract was dissolved in *n*-

hexane (100 to 300 µL) in GC vials (with inserts). Alternatively, dried extracts were separated on thin layer chromatography (TLC) plates (Merck $60F_{254}$) using dichloromethane as a developing solvent. One run of TLC yielded resolved fractions of free sterols at $R_f = 0.14$ and at sterol esters (of fatty acids) at $R_f = 0.86$. Commercial cholesterol and cholesterol oleate were used as TLC standards. Fractions containing free sterols and sterol esters were scrapped off the plate. Sterol esters were saponified as described above. Residues were then acetylated and analyzed by GC-MS. The temperature program of the oven of an Agilent 6890 chromatograph coupled to an Agilent 5973 mass selective detector included a steep ramp from 60 to 220°C (30°C.min^{-1}) then a 2°C.min^{-1} ramp from 220 to 300°C, followed by a 10 min plateau. Compounds were separated on a HP5-MS column (Agilent; 30 m long, 0.32 mm i.d., 0.25 mm film thickness; 2 mL.min^{-1} hydrogen as carrier gas) and identified by their mass spectra. Brassicasteryl acetate was detected at Rt = 34.5 min, its mass spectrum at EI 70 eV [M^+- ROH 380(100), M^+-CH3-ROH 365(5), M^+-SC-ROH 255(25)] and retention time was identical to that of an authentic standard. Total brassicasterol acetate in extracts was determined according to a standard curve.

2.8. Proteomic analyses

2.8.1. SDS-PAGE and in-gel trypsin digestion. LD fractions were prepared in biological triplicate. 8 µL of purified LD proteins adjusted to 25 µL Laemmli buffer were loaded on top of a SDS-PAGE gel (NuPAGE 4-12%, Invitrogen) and migrated on a 60 mm distance in order to separate potential lipidic front from the protein content. After Coomassie blue staining (R250, Bio-Rad), the gel areas containing proteins were manually excised and cut into 8 bands for in-gel digestion with trypsin using a Freedom EVO150 robotic platform (Tecan Traging AG, Switzerland) as follows. Gel bands were washed six times by successive incubations in NH_4HCO_3 25 mM and then in CH_3CN 50% v/v, NH_4HCO_3 25 mM. After dehydration in pure CH_3CN, reduction was carried out with DTT 10 mM in NH_4HCO_3 25 mM (45 min at 53°C) and alkylation with iodoacetamide 55 mM in NH_4HCO_3 25 mM (35 min in the dark). Alkylation was stopped by the addition of DTT 10 mM in NH_4HCO_3 25 mM (10-min incubation). Gel pieces were then washed again in NH_4HCO_3 25 mM and dehydrated with pure acetonitrile. Modified trypsin (sequencing grade, Promega) in NH_4HCO_3 25 mM was added to the dehydrated gel pieces for incubation at 37 °C overnight. Peptides were extracted from gel pieces in three sequential extraction steps (each 15 min) in 30 µL of CH_3CN 50% v/v, 30 µL of formic acid 5% v/v, and finally 30 µL of pure CH_3CN. The pooled supernatants were dried under vacuum.

2.8.2. Analysis of trypsin peptides by nanoliquid chromatography coupled to tandem mass spectrometry (nanoLC-MS/MS). The dried extracted peptides were resuspended in acetonitrile 5%, trifluoroacetic acid 0.1% and analyzed via online nano-LC-MS/MS (nano-liquid chromatography-tandem mass spectrometry; NCS and Q-Ex HF, Thermo Fischer Scientific). Peptide mixtures were desalted on line using a reverse phase precolumn (Reprosyl PUR C18 AQ 1.9 µm, 250 mm x 75 µm; Cluzeau) and resolved on a C18 column (Acclaim PepMap 100 C18, 3 µm bead size, 100 Å pore size, 250 mm x 75 µm, Dionex). Peptides were separated using 140-min gradients ranging from 4% to 50% acetonitrile in formic acid 0.1% in 123 min and wash to 90% and equilibration at 4% at a flow rate of 300 $nL.min^{-1}$. MS (mass spectrometry) and MS/MS data were acquired using the Xcalibur software (Thermo Fisher Scientific). The spray voltage was set at 2 kV and the heated capillary was adjusted to 270 °C. Survey full-scan MS spectra (*m/z* = 400–1600) were obtained in the Orbitrap with a resolution of 60,000 after accumulation of 1.10^6 ions (maximum filling time: 200 ms). The 20 most intense ions from the preview survey scan delivered by the Orbitrap were fragmented via collision-induced dissociation in the LTQ after accumulation of 1^{e5} ions (maximum filling time: 50 ms). Raw files were processed using MaxQuant version 1.5.8.3 [61].

2.8.3. Protein determination. Mass spectrometry spectra were searched against a compilation of the *P. tricornutum* protein database from the Ensembl Protists portal (Phaeodactylum_tricornutum.ASM15095v2.pep.all.fasta, 12,178 entries), the organellar-encoded proteins (165 entries) and the frequently observed contaminant database embedded in MaxQuant. Trypsin/P was chosen as the enzyme and 2 missed cleavages were allowed. Precursor mass error tolerances were set respectively at 20 ppm and 4.5 ppm for first and main searches. Fragment mass error tolerance was set to 20 ppm. Peptide modifications allowed during the search were: carbamidomethylation (C, fixed), acetyl (Protein N-ter, variable), and oxidation (M, variable). Minimum peptide length was set to 7 amino acids. Minimum number of peptides, razor + unique peptides and unique peptides were all set to 1. Maximum false discovery rates, calculated by employing a reverse database strategy, were set to 0.01 at peptide and protein levels. For quantification, the "Match between runs" option was activated. To evaluate the relative abundance of each protein in the LDs preparations, proteins were quantified using iBAQ [62]. Proteins that failed to be quantified in all three replicates were discarded. iBAQ values were normalized to the sum of all intensities within each replicate. Proteins were ranked according to the sum of normalized iBAQ (decreasing order) thus including missing values with iBAQ = 0. For annotations: descriptions of the proteins were

obtained from the Ensembl fasta file. This functional annotation was completed by expert annotations obtained from the corresponding gene version at JGI (https://genome.jgi.doe.gov/Phatr2 and https://genome.jgi.doe.gov/Phatr2_bd), based on the search for signal peptides, using the SignalP predictive method [63], chloroplast transit peptides, based on the ChloroP predictive method [64] and on the detection of an ASAFAP-motif specific to sequence import into secondary plastids [65]. Prediction of transmembrane helices in proteins was performed at the TMHMM Server v. 2.0 (http://www.cbs.dtu.dk/services/TMHMM-2.0) [66] and isoelectric point (IP) values were predicted using the Avg_Pi output of the standalone IPC Isoelectric Point Calculator program (http://isoelectric.ovh.org/) [67].

2.9. Western blot analyses

Immunodetection of organellar protein markers was performed on protein extracts from whole cells of *P. tricornutum* grown in nitrogen-rich and nitrogen-depleted media and from purified LD fractions. For whole cell extracts, 200 mL of *P. tricornutum* cells were either cultivated 7 days in 10N10P ESAW medium up to a cell concentration of 8 x 10^6 cells.mL^{-1} or incubated 7 days in 00N10P ESAW medium, after a 10-day growth in rich medium, up to a cell concentration of 9.10^6 cells.mL^{-1}. Cells were collected by centrifugation at 4,000 x g, 4°C for 7 minutes (Rotor A-4-44, Eppendorf). Pellets were quickly frozen in liquid nitrogen and stored at -80°C. Pellets were lyophilized and phenol extracted as described previously [68] with the addition of EDTA 50 mM, β-mercaptoethanol 2% v/v, PMSF 2 mM, and cOmplete protease inhibitor cocktail as specified by the supplier (Roche Diagnostics). A total of 15 µg of proteins from whole cell extracts and of 2 µg proteins from LDs were then resolved by SDS-PAGE on a 12% acrylamide gel before transfer to a nitrocellulose membrane. Immunodetection was performed by peroxidase-coupled detection (Clarity western ECL Substrate, Biorad). Antibodies against StLDP, Seipin, CNX, COP1, PEX3, ACL1, CGI-58, RAE1 and TPT1 were obtained by rabbit immunization (Biotem). Antibodies were affinity purified on the peptides. The purity of LD fraction was also checked with commercial antibody (Agrisera): Sec21p (AS08 327), PsaC (AS10 939), PsbA (AS05 084) and ATPβ mitochondrial and chloroplastic (AS05 085). All the antibodies were used at a dilution of 1/1000 with the exception of CNX at 1/5000 and ATPβ at 1/2000.

2.10. Transmission electron microscopy

For whole cell imaging, cells of *P. tricornutum* were harvested at late logarithmic phase (2 x 10^6 cells.mL^{-1}) before the offset of the light period, by centrifugation at 5,000 x g, 4 °C for 10

minutes. Cells were then fixed in glutaraldehyde 2.5% (TAAB); formaldehyde 2% (Polysciences); cacodylate 0.1 M (Sigma-Aldrich), pH 7.4, for 1 h at room temperature. Electron microscopy observation was performed using a Zeiss NVision 40 dual-beam microscope as described previously [47, 69]. For lipid droplet imaging, diluted suspensions of purified fractions were deposited onto glow-discharged carbon-coated TEM grids. After a few minutes, the liquid in excess was blotted with filter paper and, prior to drying, the preparation was negatively stained with 2% uranyl acetate. The stain in excess was blotted and the specimen was allowed to dry. Images were recorded with a Philips-FEI CM200 microscope operating at 200 kV and equipped with a TVIPS TemCam F216 digital camera.

2.11. Statistical Analysis

All the analytical determinations were performed in biological triplicate. Statistical analyses were achieved using GraphPad prism software (GraphPad solfware Inc., CA, USA). One-way and two-way ANOVA followed by Dunnett's post hoc test was carrying out. The difference between groups was considered significant when the p-value was equal to or less than 0.05.

2.12. Accession numbers

Phatr3_draftJ1735; Phatr3_draftJ977; Phatr3_EG00979; Phatr3_EG01955; Phatr3_EG01984; Phatr3_EG02298; Phatr3_EG02301; Phatr3_EG02323; Phatr3_EG02389; Phatr3_EG02643; Phatr3_J13587; Phatr3_J13662; Phatr3_J13951; Phatr3_J14618; Phatr3_J14792; Phatr3_J15138; Phatr3_J15806; Phatr3_J17545; Phatr3_J1884; Phatr3_J20657; Phatr3_J20885; Phatr3_J21122; Phatr3_J21239; Phatr3_J21929; Phatr3_J22006; Phatr3_J22122; Phatr3_J22357; Phatr3_J22395; Phatr3_J22873; Phatr3_J24820; Phatr3_J24978; Phatr3_J25743; Phatr3_J26290; Phatr3_J26921; Phatr3_J27118; Phatr3_J27518; Phatr3_J27976; Phatr3_J28737; Phatr3_J29260; Phatr3_J29702; Phatr3_J30315; Phatr3_J30486; Phatr3_J30519; Phatr3_J30660; Phatr3_J34971; Phatr3_J35766; Phatr3_J40880; Phatr3_J41856; Phatr3_J42434; Phatr3_J44488; Phatr3_J45510; Phatr3_J45679; Phatr3_J45813; Phatr3_J46098; Phatr3_J46448; Phatr3_J48778; Phatr3_J48859; Phatr3_J49286; Phatr3_J49287; Phatr3_J4937; Phatr3_J49943; Phatr3_J50214; Phatr3_J50215; Phatr3_J50236; Phatr3_J50705; Phatr3_J50872; Phatr3_J51058; Phatr3_J51066; Phatr3_J51128; Phatr3_J51157; Phatr3_J51230; Phatr3_J51305; Phatr3_J54019; Phatr3_J54086; Phatr3_J54360; Phatr3_J54534; Phatr3_J54642; Phatr3_J54686; Phatr3_J55010; Phatr3_J55230; Phatr3_J6847.

3. Results

3.1. Lipid droplet purification

LDs were purified from *P. tricornutum* wild-type cells (CCMP632/CCAP 1055/1; Pt1) cultivated in 3-liter batches in a rich medium (ESAW 10N10P) and subjected to a starvation in nitrogen (ESAW 00N10P) during seven days (Fig. 2, A1). Nitrogen starvation triggered the accumulation of LD within cells (Fig. 2, B1). We first sought to optimize the LD purification procedure previously described [49] so as to avoid contaminations by cellular debris. Cells were broken gently using a cell disruptor set at a pressure of 2 kbar. In confocal microscopy, Nile red-stained LDs appeared mixed with cell debris, including broken chloroplasts, assessed by chlorophyll fluorescence (Fig. 2, A2 and B2). We then repeated the purification procedure described previously [49], by adjusting the sucrose concentration of the broken cells to 0.25 M, loading this sample on top of a 0.7 M sucrose cushion and proceeding with an ultracentrifugation at 50,000 x g for 20 min at 4°C. The SDS PAGE analysis of the obtained fraction showed a profile similar to that described by Yoneda et al. (2016). Nevertheless, LD collected at the upper surface of the tubes were not totally separated from lower density cell debris, as lipidomic profile indicated a strong contamination by MGDG and proteomic analyses returned > 1,800 proteins in this fraction (data not shown). We sought therefore to improve this purification method, by loading the broken cell sample at the bottom of the density gradient [70, 71]. We adjusted the sucrose concentration to 1.25 M, and loaded this sample (4.5 mL) under a discontinuous gradient made of 0.7 M (7 mL) and 0.25 M sucrose (1.5 mL) layers (Fig. 2, A3). The fractionation was then achieved based on the buoyancy of low-density LDs. The 0.7 M layer also contained Triton-X100 so as to wash the surface of LDs, while moving toward the upper surface of the discontinuous gradient. After a 16-hour ultracentrifugation at 68,000 x g at 4°C, LDs were collected at the surface of the tubes, clearly separated from higher density debris (Fig. 2, A3). LD enrichment was monitored after cell disruption and after ultracentrifugation by confocal microscopy, based on Nile red staining (Fig. 2, B3). Electron microscopy negative staining of purified LDs showed exclusively spherical structures with diameters of ~100-300 nm (Fig. 2, C). This LD purification procedure was therefore used for three independent replicates and obtained LD fractions were used for further analyses.

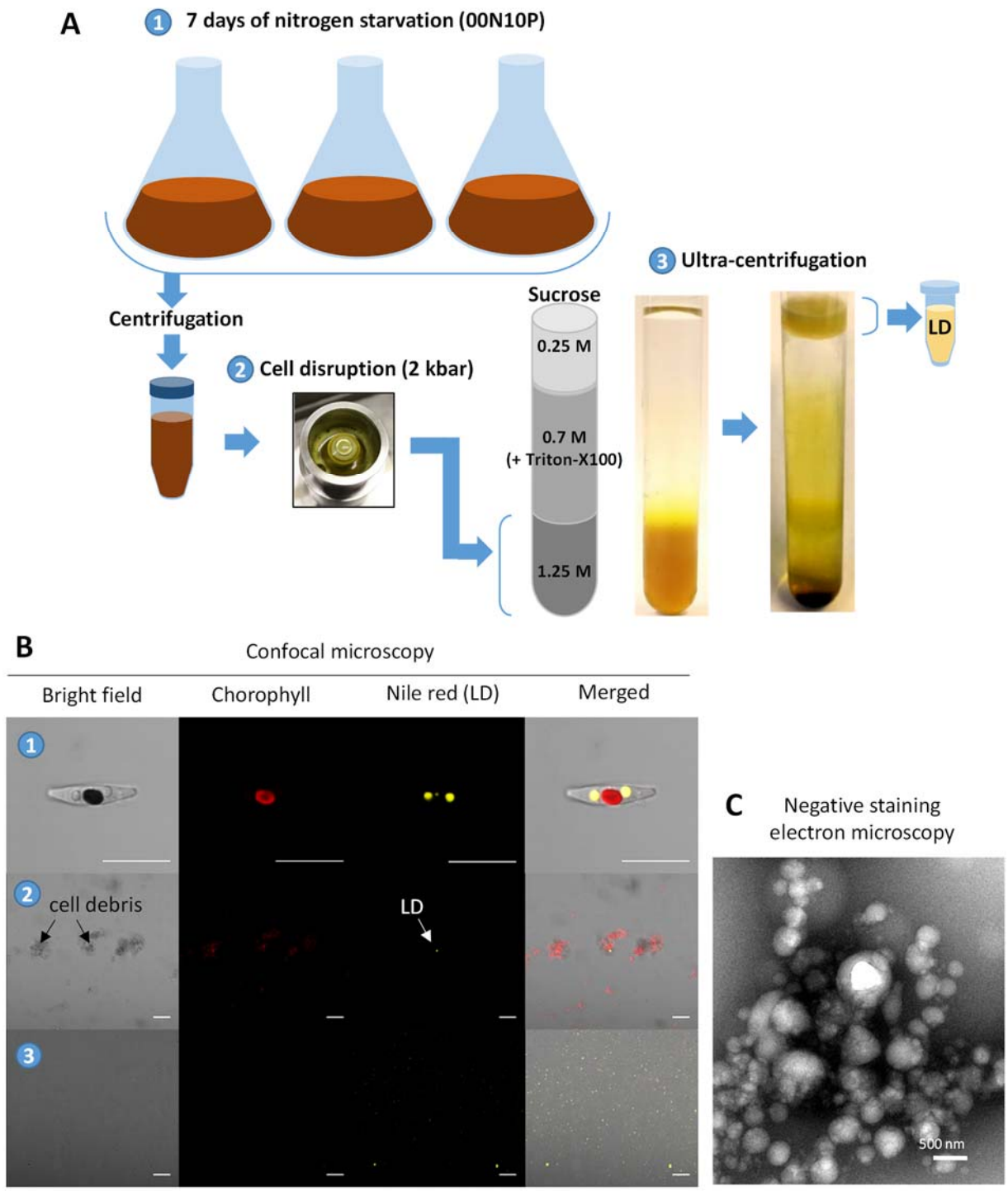

Figure 2: LD purification from nitrogen-starved *P. tricornutum* cells. A. Main steps of the LD purification protocol. *P. tricornutum* cells starved for 7 days in a medium without nitrogen (ESAW 00N10P) (step 1). Cells were collected by centrifugation and broken by high pressure (step 2). The purification was carried out by adjusting the sucrose content of the broken cells to 1.25 M prior loading 4.5 mL at the bottom of a density gradient. A 7-mL layer containing 0.7 M sucrose and triton X-100 was added, so as to allow lower density organelles to be separated based on buoyancy, while weakly associated structures and proteins were washed away by the detergent. A 1.5-mL layer containing 0.25 M sucrose was then added at the top of the tube for LD complete purification. The tubes were centrifuged at 68,000 x g, 4°C for 16 hours and purified LDs were collected at the top of the gradients (step 3). **B, Monitoring of LD enrichment by confocal imaging.** Scale bars: 10 µm. **C, Purified LDs observed by negative staining electron microscopy.** Scale bar: 500 nm. Purified LD were analyzed from three independent biological replicates.

3.2. Glycerolipidome of *P. tricornutum* lipid droplets

The glycerolipid composition of purified LDs was compared to the whole-cell glycerolipidome determined from *P. tricornutum* grown in nitrogen starvation (Fig. 3). Starved cells contained about 27 mol% of TAG, consistently with previous works [14, 17]. Most abundant polar lipids were three plastid glycoglycerolipids, *i.e.* monogalactosyldiacylglycerol (MGDG, 43.8 mol%), digalactosyldiacylglycerol (DGDG, 11.7 mol%) and sulfoquinovosyldiacylglycerol (SQDG, 7.3 mol%). Phosphatidylcholine (PC, 5.5 mol%) and the betaine lipid diacylglycerylhydroxymethyl-*N*,*N*,*N*-trimethyl-*β*-alanine (DGTA, 1.1 mol%) usually synthesized in the ER, were less abundant (Fig. 3, A). The fraction of purified LDs contained 99.0% of TAG. MGDG represented less than 0.05 mol% of LD lipids, confirming the high purity of the obtained fraction (Fig. 3, A). No diacylglycerol could be detected in LDs (Fig. 3, A) and the profile of TAG molecular species in the purified fraction was identical to that in whole cells (Fig. 3, B), indicating that the integrity of LDs was not affected by lipases after cell breakage and separation on density gradient.

We detected DGTA (0.4 mol%), SQDG (0.35 mol%) and PC (0.15 mol%) in the LD (Fig. 3, A). LDs contained nearly exclusively DGTA with eicosapentaenoic acid (C20:5) paired with palmitoleic or palmitolenic acids (C16:1 or C16:2), whereas whole cell DGTA contained also C16:0, all the C18:1, C18:2, C18:3 and C20:4 precursors of C20:5, as well as docosahexaenoic acid, C22:6 (Fig. 3, C and D). PC and SQDG occurring in LD fractions had no significant difference in their fatty acid profiles compared to whole cell extracts (Fig. 3, E and F). Whereas the presence of less than 0.05% of the major plastid lipid, MGDG, indicated a remarkably low contamination by broken chloroplasts, the presence of SQDG indicates that this plastid lipid was specifically enriched at the surface of the LD.

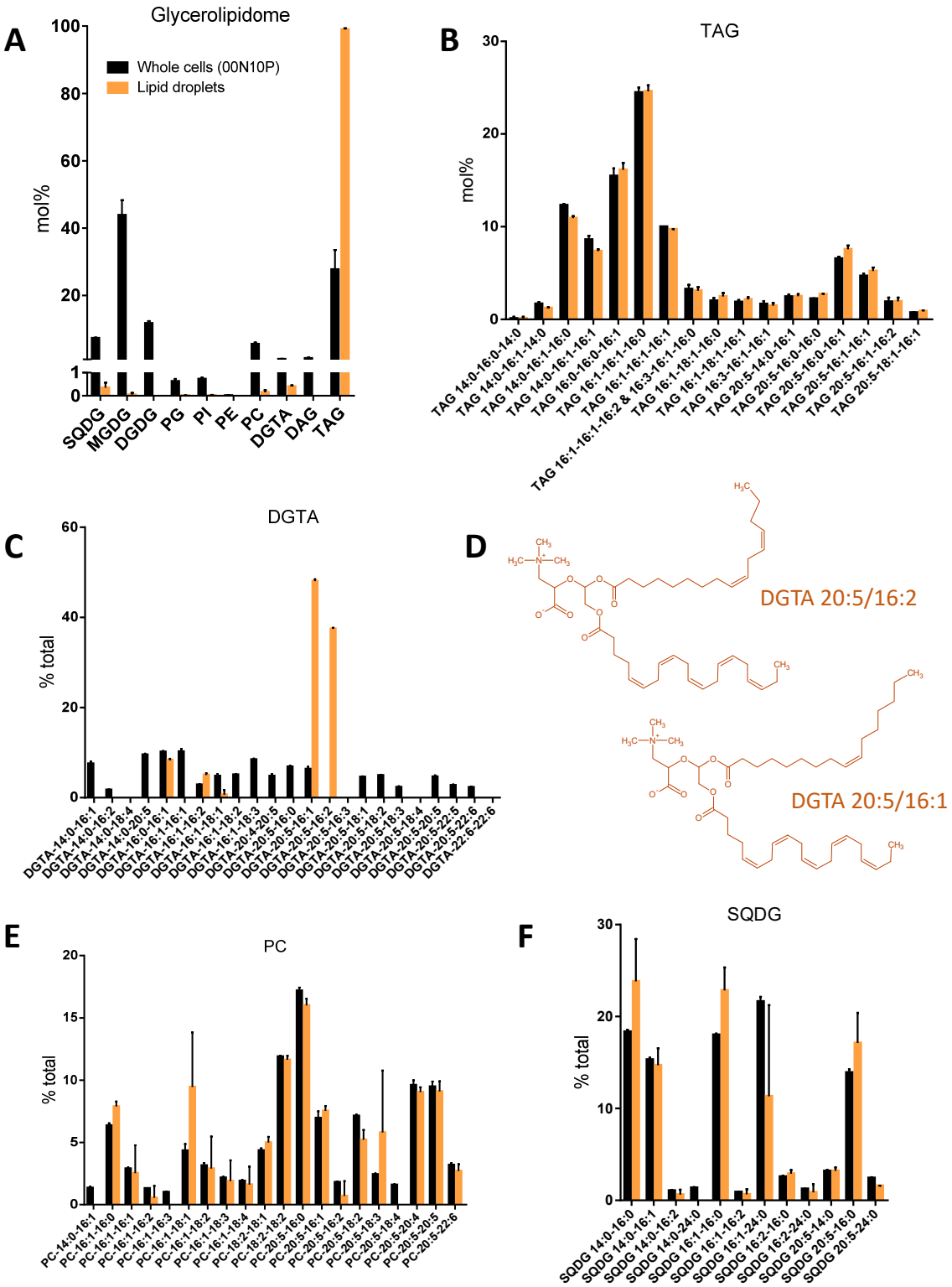

Figure 3: Glycerolipids in *P. tricornutum* lipid droplets. Glycerolipids were extracted from whole cells cultivated in nitrogen starved medium (00N10P) and from lipid droplet (LD) purified fraction. **A, Glycerolipid proportions in whole cells and purified LDs. B, TAG acyl profiles. C, DGTA acyl profiles. D, Chemical structures of the two major molecular species of DGTA in purified LDs. E, PC acyl profiles. F, SQDG acyl profiles.** Glycerolipids and molecular species are expressed in mol%. Data correspond to biological triplicates +/- standard deviation. DGDG, digalactosyldiacylglycerol; DGTA, 1,2-diacylglyceryl-3-O-2'-(hydroxymethyl)-(*N*,*N*,*N*-trimethyl)-*β*-alanine; MGDG, monogalactosyldiacylglycerol; PC, phosphatidylcholine; PE, phosphatidylethanolamine; PG, phosphatidylglycerol; PI, phosphatidylinositol; SQDG, sulfoquinovosyldiacylglycerol. Data obtained from whole cell extracts after cultivation in nitrogen depleted condition (00N10P) and from purified LDs are shown in black and orange, respectively.

3.3. A unique sterol in *P. tricornutum* lipid droplets, brassicasterol

Two major sterols have been previously identified in whole cells of *P. tricornutum*, *i.e.* brassicasterol (24-methylcholest-5,22-dien-3*β*-ol) and campesterol (24-methylcholest-5-en-3*β*-ol), with structures confirmed by mass spectrometry [72, 73]. Brassicasterol and campesterol are structurally similar to cholesterol, containing 4 strongly hydrophobic hydrocarbon rings, a hydroxyl group at the 3-carbon atom of the A-ring and a short alkyl tail: these molecules display therefore amphipathic properties [74]. Here, we clearly identified one single molecular species, brassicasterol, in whole cells extracts and in purified LD fractions (Supplemental Fig. S1), representing less than 5 mol% of total sterols + glycerolipids. Structure was assessed by mass spectrometry based on the identification of brassicasteryl specific fragments with m/z of 255.2 [M^+-SC-ROH], 365.0 [$3M^+$-CH3-ROH] and 380.4 [M^+- ROH]. Remarkably, we could not detect any brassicasterol ester but only free brassicasterol as a pathway end-product. This low proportion of such an amphipathic lipid indicates that it is located close to, or inside the lipid monolayer at the surface of the LD and not in the hydrophobic core [75, 76].

3.4. Specific enrichment of lipid droplets in *β*-carotene

Purified LDs floating at the surface of the density gradient had a pale yellow color, whereas dense cell debris, at the bottom of the tube, were brown (Fig. 2A). We addressed the possible accumulation of pigmented carotenoids within LDs. Fucoxanthin is one of the main pigments in *P. tricornutum*, cultivated in either rich or nitrogen depleted condition [77]. In the present cultivation conditions in nitrogen rich (ESAW 10N10P) and nitrogen depleted (ESAW 00N10P) media, fucoxanthin represents more than 40 mol% of total carotenoid and chlorophyll pigments (Fig. 4). In purified LDs, the same proportion of fucoxanthin was measured (Fig. 4), suggesting that a nonspecific enrichment of this hydrophobic molecule might have occurred in the course of LD purification. However, whereas whole cells also contained high levels of diadinoxanthin, chlorophyllide *a* and chlorophylls *a* and *c*, only traces of these pigments could be detected in the LD enriched fraction, further supporting the high purity level of the obtained fraction. By contrast, LDs were strongly enriched in *β*-carotene representing 28.7 mol% of total LD pigments (Fig. 4). Since this carotenoid is extremely minor at the whole cell level, it appears as a specific component of the LD enriched fraction of *P. tricornutum*.

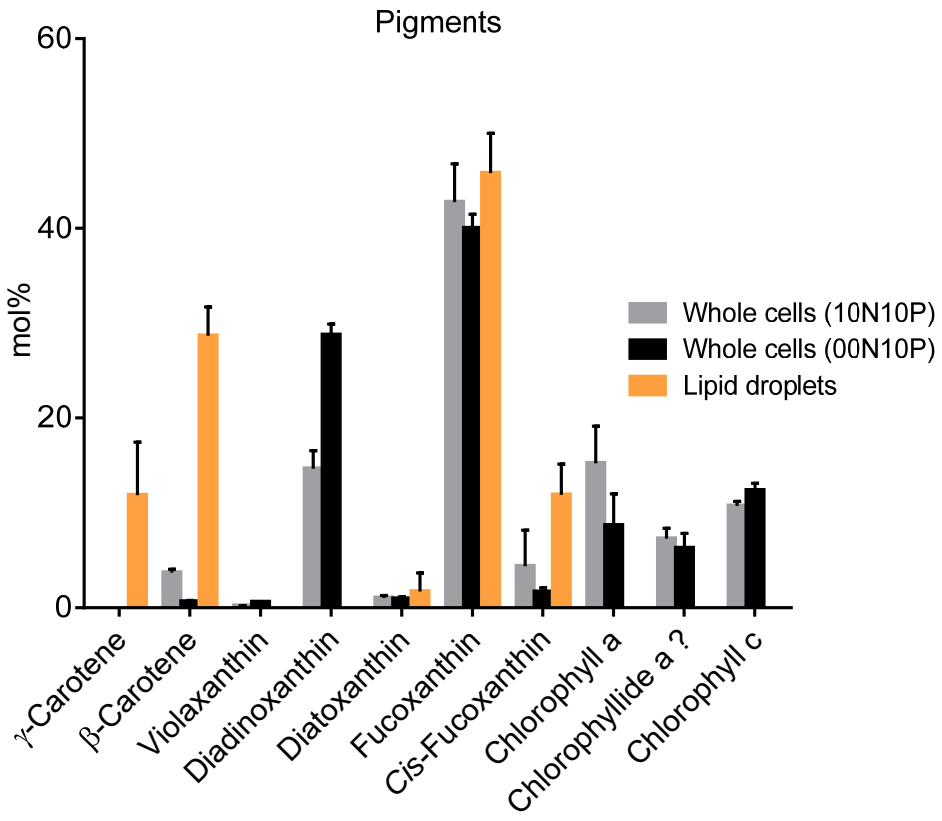

Figure 4: Carotenoids in *P. tricornutum* lipid droplets. Carotenoids and chlorophylls from whole cells and purified LDs were extracted and analyzed as described in the Methods section. Pigments from whole cells cultivated in nutrient rich condition (10N10P), nitrogen starved condition (00N10P) and in purified LDs are shown in grey, black and orange, respectively. All pigments were determined by comparison with standard molecules. Error bars, standard deviation; n = 3.

3.5. Analysis of the lipid droplet protein fractions using organelle-specific antibodies

Cross contaminations and association of subcellular organelles with purified LDs are not easy to evaluate in *P. tricornutum* samples because specific antibodies are not readily available. We have therefore developed a series of eight antibodies directed against protein markers of *P. tricornutum* cell compartments. Antigenic peptides were selected in the sequences of the Stramenopile Lipid Droplet Protein (StLDP, Phatr3_J48859) [49], a SEIPIN known to act in the initial budding of nascent LDs (SEIPIN, Phatr3_J47296) [78], a calnexin located at the ER (CNX, Phatr3_J41172), the alpha subunit of the coatomer, known to act in vesicular trafficking and to bind LDs in various systems [28] (COPA or COP1, Phatr3_J21929), the CGI-58 protein, located at the LD in mammals and at the peroxisome in plants [79-81] (CGI-58, Phatr3_J54974), a peroxisomal biogenesis factor (PEX3, Phatr3_J50623), an acyl-coA ligase 1 predicted to locate at the peroxisome (ACL1, Phatr3_J17720), a mRNA export factor binding at the nuclear pores (RAE1, Phatr3_J24439) and an isoform of triose phosphate transporter

located at the outermost epiplastid membrane, EpM (see Fig. 1) [82] (TPT1, Phatr3_J50742). We also used commercial antibodies raised against the gamma subunit of the coatomer, (Sec21p; Phatr3_J10209), plastid proteins, i.e. the D1 subunit of photosystem II (PsbA; Q5D706), an iron-sulfur protein of photosystem I (PsaC; Psac_phatc), and eventually the beta subunit of the mitochondria ATP-synthase (ATPβ chloroplastic and mitochondrial).

The yield in LDs following the procedure detailed here coupled with the protein extraction procedure used to eliminate TAG before SDS-PAGE, did not allow conventional protein quantification for the prepared samples; we therefore proceeded to an evaluation of the amount of proteins based on silver nitrate staining after SDS-PAGE separation (Fig. 5A). A known amount of *P. tricornutum* whole cell proteins (1.5 µg), obtained after cultivation in ESAW 10N10P or ESAW 00N10P media, was loaded in parallel with 2 µL of concentrated LD proteins, allowing to estimate a concentration of ~33 ng of LD proteins per µL. For Western blot analyses, we used 15 µg of whole cell proteins in parallel with 2 µg of concentrated LD proteins (Fig. 5B). We observed an increase in StLDP abundance in whole cell extracts when cells were grown in nitrogen starvation and we detected StLDP in the purified LD fraction (Fig. 5B). The antibody raised against the SEIPIN protein, acting early in the biogenesis of the LD, did not react with the purified LD fraction, suggesting that this protein was not associated with the mature LDs. For all other immunodetections, only CNX known to locate at the ER did react with the proteins extracted from purified LDs. Antibodies targeting the plastid envelope membrane, plastid thylakoids, peroxisome, mitochondria and the nuclear envelope did not react with the proteins extracted from purified LDs (Fig. 5B). In the specific case of RAE1, the protein was detected in whole cells grown in nutrient replete condition, but not upon nitrogen starvation, so the absence of reaction of the anti-RAE1 antibody with LD proteins might simply reflect the absence of the antigenic protein. Altogether, these analyses support a high level of purity of obtained LDs. The purification procedure including the floatation through a gradient containing Triton-X100 has therefore washed the surface of LDs of possible contaminants. A loss of components bridging the LD to other organelles, such as the ER, the EpM, the mitochondria and/or the peroxisome cannot be excluded.

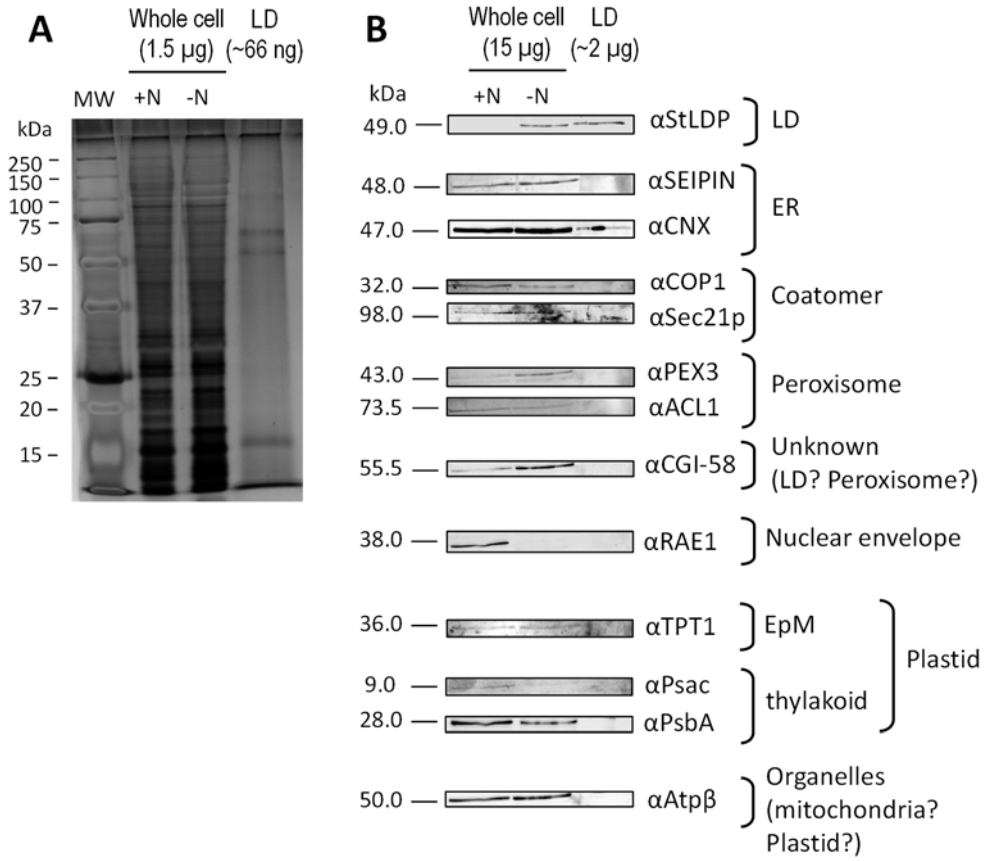

Figure 5: Western blot analysis of the LD purified fraction. A, Silver nitrate staining of whole cell and lipid droplet protein extracts. A known amount of *P. tricornutum* whole cell proteins (1.5 µg), obtained after cultivation in ESAW 10N10P (+N) or ESAW 00N10P (-N) media, was loaded in parallel with 2 µL of concentrated LD proteins. The amount of protein in the purified fraction of LDs was evaluated by comparison at ~33 ng.µL^{-1}. MW, Molecular Weight. **B, Western-blot analysis of LD protein fraction using antibodies raised against membrane compartment markers.** The purity of the LD purification was checked by using antibodies raised against different cell compartment markers: StLDP (LD), Seipin (ER), CNX (ER), COP1 and Sec21p (coatomer), PEX3 and ACL1 (Peroxisome), CGI-58 (unknown localization in *P. tricornutum*), RAE1 (Nuclear envelope), TPT1 (Plastid - EpM), PsbA (Plastid – thylakoid) and ATPβ (mitochondria and plastid). All antibodies were used at a dilution of 1/1000 except anti-CNX (αCNX) at 1/5000 and anti-ATPβ (αATPβ) at 1/2000.

3.6. Mass spectrometry-based characterization and bioinformatic analysis of the lipid droplet proteome

Proteomic analyses of LD enriched fractions were performed using three independent biological replicates (samples named LD1, LD2 and LD3). For this, proteins were in-gel digested using trypsin before analysis of the resulting peptides using nano-LC-MS/MS. Obtained spectra were identified through searches against a compilation of sequences of the *P. tricornutum* protein database from the Ensembl Protists portal (12,178 entries) and the organellar-encoded proteins (165 entries). This strategy allowed to identify 326 different proteins in total (Supplemental Table S1). In order to build up a reference proteome of LDs from *P. tricornutum*, we set up stringency filters. We first decided to only take into account

proteins highly confidently identified with a minimum of 3 peptides, selecting a sublist of 92 proteins (Fig. 6).

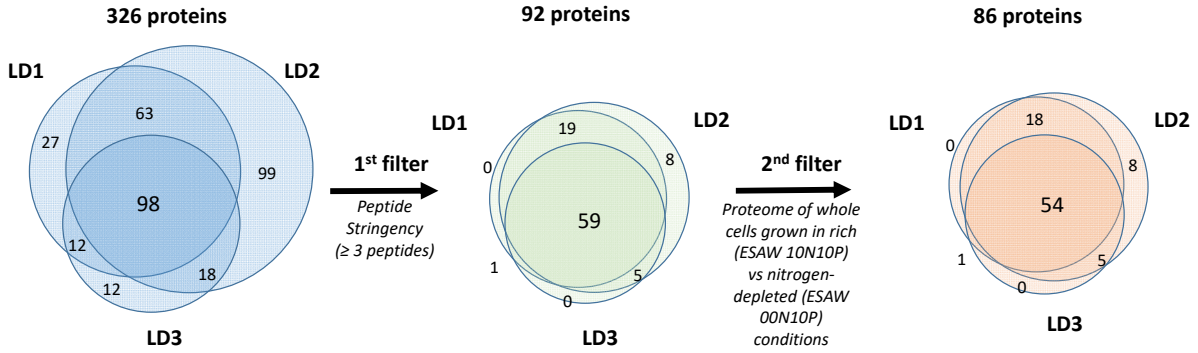

Figure 6: Characterization of *P. tricornutum* LD core proteome. Proteomic analysis led to the identification of 326 proteins from three independent biological replicates of LD fractions from *P. tricornutum*. To build a reference LD proteome, 2 different filters were then applied. The first one led to the conservation of proteins identified with at least three tryptic peptides. The second filter corresponds to a subtraction of proteins detected in whole cells downregulated in nitrogen-starved condition (ESAW 0N10P) compared to nitrogen-rich condition (ESAW 10N10P). Six proteins were removed from the proteome of purified LDs.

In order to select proteins associated with the LD specifically induced by nitrogen starvation, we applied a second filter based on proteins accumulating in whole cell extracts following a depletion of nitrogen. For this, we took advantage of results from another quantitative proteomic analysis of *P. tricornutum* whole cells, cultivated in rich (ESAW 10N10P) and nitrogen depleted (ESAW 00N10P) conditions (data not shown). We discarded from the list of LDs proteins six proteins found to be downregulated in the total proteome of nitrogen-depleted cells (Phatr3_EG01907, Phatr3_J55209, Phatr3_draftJ1806, Phatr3_J54477, Phatr3_J49151 and gi|118411023|ref|YP_874418.1| corresponding to the RUBISCO large subunit).

The LD proteome of *P. tricornutum* is presented in Table 1. First of all, we identified three of the five major proteins identified in the first proteomic study performed on *P. tricornutum* LD [49]: the Stramenopile Lipid Droplet Protein (StLDP, Phatr3_J48859) that was confirmed to localize at its surface [51], the Lipid droplet acyl CoA binding protein (LD-ACBD, Phatr3_J48778) and a Heat shock protein (HSP70A, Phatr3_J54019).

The proteome revealed the presence of proteins belonging to the PAP (Plastid lipid associated protein)/Fibrillin family. This family of proteins is found on the surface of plastoglobules [83, 84], a category of lipid bodies generated inside chloroplasts [85]. The generation of TAG-rich lipid droplets inside chloroplasts has been proposed [86], but was recently shown as very unlikely [87]. The detection of these proteins suggests therefore that a minor fraction of plastoglobules were recovered during the purification of cytosolic LDs.

Interestingly, none of the enzymes involved in TAG assembly, such as DGAT or PDAT, or in early biogenesis of the LD, such as SEIPIN, were present in the mature LD proteome. We did neither detect enzymes involved in massive hydrolysis of TAG, such as lipases, or CGI-58 known to be involved in lipogenesis in mammals and plants. The proteomic profile we obtained reflected therefore a rather stable and mature organelle. We classified the functional annotations of the 86 proteins in seven large groups: metabolism (19 proteins), membrane organelles (9 proteins), chaperones, protein folding, postranslational modifications, quality control (12 proteins), cytoskeleton (3 proteins), genetic information processing (15 proteins), plastoglobules and thylakoid components (18 proteins) and unknown proteins (10 proteins) (Table 1).

Metabolic enzymes enriched in the LD purified fraction involved mainly cytosolic enzymes of the glycolytic and pentose phosphate pathways, and mitochondrial components of the Krebs cycle (Table 1). The plastid carbonic anhydrase (Phatr3_J22357) and acetyl-CoA carboxylase (Phatr3_EG019955) indicate proximity of LDs with the initiation of fatty acid biosynthesis. Enzymes involved in the catabolism of amino acids, reallocating carbon toward lipids, were detected, *i.e.* a glutamine synthase (GS, Phatr3_J22357), glutamate dehydrogenase (GDH, Phatr3_J13951); agmatinase (AGMAT, Phatr3_J40880) and urease (UREC, Phatr3_J29702). Two important proteins involved in acyl-CoA metabolism were also found associated to LDs, *i.e.* a long chain acyl-CoA synthetase (ACS4, Phatr3_J45510) and the LD-ACBD. The presence of plastid- and mitochondria-located enzymes suggests the presence of contact sites with these organelles.

LD contact with other organelles is supported by the detection of membrane proteins, mainly from endomembranes, such as two subunits of the COP1 coatomer (COPA; Phatr3_J21929; COPBETA2, Phatr3_J27518), two components of the clathrin vesicle coating system (CHC, Phatr3_EG01984; PTAP1/2BETA, Phatr3_draftJ1735), a V-ATPase (VATPase, Phatr3_J51058) and a subunit of an ABC transporter (Phatr3_EG02323). Contact with mitochondrial envelope is supported by the detection of an adenine nucleotide translocator at the inner mitochondrial envelope membrane (SLC25A4, Phatr3_J22873). Membrane proteins from the plastid, more precisely the EpM, were not identified, but it is not excluded that some of the unknown proteins listed here might be located at the EpM. Consistently with this hypothetical localization, 5 of the unknown proteins exhibit a putative signal peptide (Phatr3_J44488, Phatr3_J50215, Phatr3_J49286, Phatr3_J50214, Phatr3_EG02301) based on the SignalP predictive method [63], one containing 3 transmembrane domains

(Phatr3_EG02301). One of the unknown proteins is predicted to contain a chloroplast transit peptide (Phatr3_J55010) based on the ChloroP predictive method [64] and on the detection of an ASAFAP-motif specific to sequence import into secondary plastids [65].

LD fraction was enriched in chaperones and components of ubiquitin-regulated machineries controlling protein folding (Table 1). The translation of mRNA into proteins at the periphery of LDs appears therefore facilitated, and is further supported by the presence of 40S and 60S ribososmal subunits and three components of RNA translation machinery, *i.e.* Elongation factors 1-alpha and 2 (EF1A, Phatr3_J28737; EF2, Phatr3_J35766) and the Eukaryotic translation initiation factor 4A (EIF4A, Phatr3_J25743). Ribosomes are often considered as non-specific contaminants, but the detection of the complete flow from protein synthesis to folding and quality control appears as significant.

Eventually, the LD fraction was also enriched in four histone isoforms (H2B-1B, Phatr3_J54360; H3-1C, Phatr3_J50872; H3.3, Phatr3_J21239; H4-1B, Phatr3_J34971), a feature previously described in LDs from Drosophila embryos [88]. Histone association to LDs pauses the question of a possible role of this organelle in the storage of some specific proteins, mainly histones, in a context where most proteins are degraded.

4. Discussion

4.1. Purity of the *P. tricornutum* LD fraction

A protocol for *P. tricornutum* LD purification has been described previously, by loading broken cells on top of a discontinuous gradient, followed by an ultracentrifugation so as to pellet higher density cell components [49]. We adjusted this first protocol to reduce contamination to a minimum. A possible alternative is to load broken cells at the bottom of the centrifugation tube, under a discontinuous gradient [70, 71, 89]. We therefore adjusted the broken cell suspension to 1.25 M sucrose and loaded this sample under a 0.7 M-sucrose layer containing Triton X-100. The addition of detergent aimed at washing the low-density LDs from contaminants and large cell debris, while moving to the top of the tube based on their buoyancy. This process might possibly remove weakly bound LD components, which might be lost in our analysis. A 0.25 M-sucrose layer was added at the top for the recovery of LD, without detergent. After 16 hours of ultracentrifugation at 68,000 x g at 4°C, LDs were clearly separated from cellular debris as assessed by confocal and electron microscopy (Figure 2). With 99 mol% of TAG and a barely detected amount of MGDG (Figure 3), the LD fraction presented a high purity. We could also immunodetect the Stramenopile LD protein (StLDP), the only known marker of *P. tricornutum* LD [49, 51] in the LD enriched fraction, whereas none of the antibodies raised against other cell compartments could cross-react with LD protein extracts, with the notable exception of an anti-calnexin (αCNX) (Figure 5). Based on the antibody specificity, a lack of immunodetection might indicate an absence of the antigenic protein or a very low proportion compared to the main pool of this protein in another location of the cell. It is apparently contradictory that the COP1/COPA coatomer subunit could not be immunodetected in the LD fraction, whereas it was detected in the proteomic analysis performed on the same sample. The sensitivity of proteomic approach proved to be higher than the antibody we have developed, and the portion of COP1/COPA associated to LDs is likely much lower than that in other organelles, such as in the set of trafficking vesicles.

We observed a pale yellow color of the purified LD fraction, suggesting the presence of specific pigments. No significant difference was observed for fucoxanthin between total extracts and purified LD fraction (Figure 4). However, chlorophylls a and c, which are parts of fucoxanthin-chlorophyll protein complexes (FCP) [90, 91] were only detected in the total extracts and in very small proportion in the purified fraction. The fucoxanthin molecules we detected therefore belong to a distinct pool. The presence of other low-density lipid bodies from the stroma of the plastid is evidenced, since we detected marker proteins of plastoglobules, i.e. plastid lipid-

associated protein (PAP) fibrillins (PAPFIB, Phatr3_J45813 and Phatr3_J49943) (Table 1). Plastoglobules are particular lipid bodies generated in the chloroplast, and could contain carotenoids. Their presence in the LD fraction cannot be avoided by a separation method based on density. They explain why some internal components of the plastid occur in the purified LD fraction, easily identified in the obtained proteome (about 20 proteins, out of 86, see below). The presence of plastoglobules, even in very minor amount, makes it difficult to assess whether the obtained carotenoid profile is strictly associated to the cytosolic LD or to these plastid lipid bodies. The unresolved localization of observed fucoxanthin also applies to *β*-carotene, however the presence of this carotenoid in plastoglobules is unlikely and comparison with other eukaryotes supports its presence in cytosolic LDs in *P. tricornutum*.

4.2. A hydrophobic core containing triacylglycerol and devoid of steryl esters

TAG making the bulk of *P. tricornutum* LD are localized in the hydrophobic core of the organelle. The composition of acyl molecular species in TAG did not differ from that in total extracts (Figure 3) confirming that no undesired hydrolysis had occurred in the course of LD purification. We addressed the presence of other hydrophobic molecules, such as steryl esters, as reported in other eukaryote models [28-30], but we could not detect the presence of any such molecule. As discussed above, the hydrophobic core could also be enriched in fucoxanthin, at the end of synthesis of carotenoids and *β*-carotene (Figure 4). The presence of pigments in cytosolic LDs has been described previously in the green alga *Haematococcus pluvialis.* In *H. pluvialis* astaxanthin (a red ketocarotenoid) is synthesized from *β*-carotene by the action of a *β*-carotene ketolase, when environmental conditions become unfavorable [92, 93]. One model proposes an export of *β*-carotene from chloroplast to the ER, where it could be converted into astaxanthin, then astaxanthin ester and stored in LD [43, 93-95]. In *P. tricornutum* a similar model might be proposed, based on an export of *β*-carotene from the plastid to the ER or the epiplastid membrane. A gene encoding a putative lycopene cyclase (Phatr3_J8835) can be detected in the genome of *P. tricornutum*. However, the corresponding protein was not detected in the LD proteome, raising questions about its location and function.

4.3. A limiting monolayer containing sulfoquivovosyldiacylglycerol, phosphatiodylcholine, brassicasterol and specific molecular species of the betaine lipid

The glycerolipidome of *P. tricornutum* LD contains 0.4 mol% of DGTA, 0.35% of SQDG and 0.15% of PC. Based on the glycerolipid profile of whole cells, dominated by MGDG, the presence of only traces of this galactolipid highlights that detected polar lipids are not

contaminants but actual components of the monolayer encapsulating LDs. The presence of SQDG, usually restricted to plastid membranes [5] is therefore remarkable and suggests that the membrane at the origin of the LD in *P. tricornutum* should contain this lipid. By contrast, PC [96] and betaine lipid [97] are usually synthesized in the ER. PC is a glycerophospholipid frequently found in the LD monolayer of several study models, such as mammals [98] or yeasts such as *Saccharomyces cerevisiae* [75, 99] and *Pichia pastoris* [100]. PC is known to relocate to the outer leaflet of the outer envelope membrane in primary chloroplasts [101], so it is possible that part of PC lies in the outermost membrane of the plastid in *P. tricornutum*. Eventually, brassicasterol is detected in purified LDs. Sterols are usually restricted to endomembranes and absent from plastids. Nevertheless, they have been detected in the non-photosynthetic secondary plastid in the Apicomplexa *Plasmodium falciparum* [102], and similarly, brassicasterol could also be localized in *Phaedoactylum* plastid membranes.

The precise composition of the four membranes limiting diatom's plastid has not been determined to date [5]. The hybrid presence of a plastid lipid (SQDG) and ER lipids (DGTA, PC, brassicasterol) we report here, supports therefore that the membrane producing LDs is the outermost membrane of the plastid, the epiplastid membrane (EpM). A major question raised by our results is the origin of SQDG in the EpM, either following an export from a site of synthesis within the plastid, or the presence of a synthesis pathway in the EpM.

DGTA is a betaine lipid, a class of glycerolipids, which is not conserved in the evolution of eukaryotes, having two fatty acids esterified in the *sn*-1 and *sn*-2 position and a betaine group connected by an ether bond in the *sn*-3 position (Figure 3). Three betaines lipid are described in the literature: 1,2-diacylglyceryl-3-O-2'-(hydroxymethyl)-(*N*,*N*,*N*-trimethyl)-*β*-alanine (DGTA), 1,2-diacylglyceryl-3-O-4'-(*N*,*N*,*N*-trimethyl)-homoserine (DGTS) and 1,2-diacylglyceryl-3-O-carboxy-*(*hydroxymethyl)-choline (DGCC). In phosphate deficiency, betaine lipids accumulate in many organisms including diatoms [14, 103]. Phosphate starvation leads to a degradation of phospholipids, releasing phosphate for recycling purposes, and current models propose that betaine lipids could compensate the subsequent lack of phospholipids [104]. In systems like diatoms, and based on the present study, betaine lipids could also help in LD biogenesis.

Two molecular species of DGTA are strikingly enriched in *P. tricornutum* LD, with a very simple fatty acyl profile, *i.e.* containing eicosapentaenoic acid paired with palmitoleic or palmitolenic acids, DGTA 20:5/16:1 and DGTA 20:5/16:2 respectively. The betaine lipid is considered as a platform to synthesize C20:5 very-long chain polyunsaturated fatty acids (VLC-

PUFAs), as evidenced by the presence of fatty acid precursors, *i.e.* C18:1, C18:2, C18:3 and C20:4 in DGTA [24, 105-107]. The DGTA molecular species of LDs do not contain these precursors and are therefore sorted downstream C20:5 biosynthesis. Their synthesis should therefore occur in another subcellular location, likely in ER membranes disconnected from the EpM. Furthermore, in the lipidome of *P. tricornutum*, C16:2 is mainly present in MGDG and DGDG and seems absent from ER glycerolipids [14]. The detection of this fatty acid in this pool of DGTA supports an origin from the plastid.

The biosynthetic pathway of betaine lipids was reported only for DGTS in the *Chlamydomonas reinhardtii* and *Nannochloropsis oceanica* models [108, 109], and involves a betaine lipid synthase (BTA1). A BTA1 homologue, called BTA1-Like (Phatr3_J42872) has been identified in *P. tricornutum* [20, 109]. In two recent transcriptomic studies of *P. tricornutum* exposed to stress leading to TAG accumulation, i.e. following exposure to nitric oxide [20] and to 17α-ethynylestradiol, a derivative of the natural estrone and estradiol hormones [24], the gene encoding the BTA-like enzyme was upregulated. In the case of 17α-ethynylestradiol treatment, the overexpression of the betaine lipid synthase coincided with the disruption of the very-long chain polyunsaturated fatty acid synthesis, marked by a decrease of eicosapentaenoic acid (20:5) and an increase in precursor fatty acids (C18:2, C18:3 and C18:4) [24]. We did not find any data regarding the level of expression of BTA1-Like in transcriptome datasets of *P. tricornutum* following nitrogen deficiency [110, 111] and the expression of this gene should therefore be investigated in the future to assess whether its expression correlates with LD biogenesis in all known conditions.

Brassicasterol (24-methylcholest-5,22-dien-3β-ol) is the final product of the sterol biosynthesis pathway in *P. tricornutum* [73]. Sterols and TAG share a common starting point in their biosynthesis, acetyl-CoA, also used for the synthesis of fatty acids in the plastid. Sterols and TAG are therefore in competition with respect to carbon allocation. This was illustrated by either genetic or chemical impairment of sterol synthesis leading to an increase in TAG [24, 73]. Based on the polarity of brassicasterol and on its proportion in LD (< 5 mol% brassicasterol, compared to sterol + glycerolipids), we suppose that this free sterol is at the periphery and in the polar lipid monolayer of the LD.

4.4. A proteome indicating a proximity with the endomembrane system

Among the set of 86 proteins (Table 1), we detected six proteins involved in endomembrane trafficking. We first detect two coatomer proteins in the purified lipid LD fraction, COPA (Phatr3_J21929) and COPBETA2 (Phatr3_J27518). These two proteins are part of the COP1

complex. This complex is composed of seven subunits (α, β, β', γ, ε, δ, ζ) and participates in the retrograde transport of vesicles from *trans*-Golgi network to endoplasmic reticulum and in *intra*-Golgi transport [112]. In the unfiltered initial proteome (326 proteins), two other components of the coatomer were present (COPBETA, Phatr3_J54511; and COPGAMMA, Phatr3_J10209) (Supplemental Table 1). Based on the lack of immunodetection of COPA in the LD fraction using an anti-COP1 antibody reacting with proteins from whole cell extracts (Figure 5), we deduce that only a small fraction of cell COP1 is associated with LD, whereas the rest is likely associated with retrograde vesicles. In *Drosophila*, the COP1 protein complex regulates the composition of perilipines on the surface of the LD and promotes the association of Adipose Triglyceride Lipase (ATGL) on the surface of the LD to initiate lipolysis [113]. Four subunits (α, β, γ_1 and γ_2) of COP1 were also found in the LD proteome of mouse testicular Leydig cells [114]. The complex COP1 is dependent on the presence of ARF1 for its operation [115]. Using an *in vitro* system, the ARF1/COP1 machinery was shown to allow the synthesis of nano LDs of 60 to 80 nm in mammalian cells, acting therefore in LD homeostasis [116]. In this study, ARF1/COPI proteins not only localize to LDs to bud nano-LDs, but they are required for targeting specific TAG-synthesis enzymes to LD surfaces. In the unfiltered set of 326 proteins identified in *P. tricornutum* purified LDs, we identified 5 small GTPases (ARF1, Phatr3_J43251; RAB1A, Phatr3_J22713; RABX1, Phatr3_draftJ998; RAN1, Phatr3_J51169 and Phatr3_J36721), including ARF1, suggesting that a similar machinery might operate at the periphery of LDs, possibly controlling the budding of nano-LDs and/or addressing specific enzymes to its surface.

The proteome of *P. tricornutum* LD also highlights two proteins involved in the formation of clathrin, i.e. clathrin heavy chain (CHC, Phatr3_EG01984) and the beta subunit of clathrin adaptor complex AP2 (Phatr3_draftJ1735) (Table 1). The alpha subunit of clathrin adaptor complex AP2 (AP1 alpha, Phatr3_J54442) was detected in the unfiltered proteome (Supplemental Table 1). Clathrins participate in protein transfer outside the *trans* Golgi network [117]. AP1 is involved in autophagosome formation from *trans* Golgi network [118]. The presence of these components further supports a connection with specific cytosolic vesicles. In the unfiltered proteome, we also identified 5 SNARE (Soluble N-ethylmaleimide-sensitive-factor Attachment protein REceptor) proteins (Supplemental Table 1). SNARE proteins are necessary for fusion of transport vesicles with target membranes [119]. These proteins are notably involved in the COP1 transport as well as in the autophagy mechanism. The SNARE proteins are divided into two categories: R-SNARE (formerly v-SNARE, v for vesicle) and Q-SNARE (formerly t-SNARE, t for target). Fusion between two membranes is favored by the

formation of a four-helix bundle composed of one R-SNARE and three Q-SNARE [120]. R corresponds to the addition of an arginine during the fusion whereas Q corresponds to the addition of a glutamine. Of the five SNAREs detected, only one corresponds to a Q-SNARE (Syntaxin-61, Phatr3_EG02404). The other four proteins are R-SNARE (VAMP72, VPS9D1, VPS41 and VPS). VPS proteins are involved in the docking of vesicles to their target membrane [119]. Three other proteins detected in the unfiltered LD proteome are also involved in mechanisms of autophagy and clathrin formation, two annexins (ANX, Phatr3_J44109 and ANXA1, Phatr3_J54190) completing the nonaspanin (TM9SF, Phatr3_J13662) detected in the filtered set. A recent study of *P. tricornutum* proteome highlighted an increase in endocytosis and phagosomal activities in nitrogen depleted conditions [121]. The uncharacterized membrane compartment observed by electron microscopy in the vicinity of *P. tricornutum* LDs shows vesicles inside a membrane sack and could possibly correspond to an autophagosome, as observed in other cell types [122, 123] (Fig. 1, indicated by a star). The role of these components at the periphery of LDs should therefore be addressed in future works.

We detected a Vacuolar-Type H^+-ATPase (Phatr3_J51058) in the filtered list and 6 additional V-ATPases in the unfiltered one (Phatr3_J10862, Phatr3_J27923, Phatr3_J29711, Phatr3_J15844, Phatr3_J28794 and Phatr3_J21030). V-ATPases correspond to a family of proton pumps using hydrolysis of ATP to produce a proton gradient in endomembrane vesicles and compartments. This kind of pump is usually found in secretory vesicles as well as in endosomes and lysosomes [124]. A V-ATPase was previously detected in the proteome of the alkenone body (a particular LD storing very long chain ketones) of *Tisochrysis lutea* [125]. Together with components of the endoplasmic-reticulum-associated protein degradation (ERAD) pathway located in the ER (see below), the proteome of *P. tricornutum* LDs suggests tights connections with different compartments of the endomembrane system (ER, Golgi, Trans-Golgi, trafficking vesicles, clathrin-coated vesicles), consistently with contacts observed by electron microscopy (Figure 1). The structure and function of these contact sites now need to be structurally and functionally characterized.

4.5. A putative site for mRNA storage and a platform for specific synthesis and folding of proteins, coupled with the ERAD quality control system

The *P. tricornutum* LD proteome contains four proteins involved in post-translational modifications such as ubiquitination (UBI3 - Phatr3_J27118 and PUB39 - Phatr3_J46098) and phosphorylation (STK - Phatr3_J45679 and EPK2 – Phatr3_EG02389). Ubiquitination was previously shown to be a significant post-translational modification controlling lipolysis in plants [126]. Oleosins on the surface of the oleaginous seed LDs are thus ubiquitinated by the

attachment of distinct ubiquitin motifs (monoubiquitin Ub, K48-linked diubiquitine $K48Ub_2$ and K63-linked diubiquitin $K63Ub_2$) allowing addressing this protein to the 26S proteasome in the cytosol for its degradation [127]. It has been recently shown, by two independent teams, in the pollen tube of *Nicotiana tabacum* and in germinating seedlings of *Arabidopsis thaliana*, that the protein PUX10 (Plant UBX Domain-containing Protein 10), located on the surface of LDs, participated in the recognition of polyubiquitinated K48 motifs with its UBA domain [127, 128]. PUX10, via its UBX domain, recruits the AAA-type ATPase Cell Division Cycle 48 protein (CDC48), a protein involved in the ERAD (Endoplasmic-reticulum-associated protein degradation) pathway. CDC48 is a protein that facilitates the transfer of polyubiquitinated misfolded protein to the 26S proteasome. Interestingly, the CDC48 (Phatr3_J54642) protein is present in *P. tricornutum* LD proteome (Table 1). A second protein involved in the ERAD pathway has also been detected, an ER luminal binding protein (BIP - Phatr3_EG02643), further supporting the association of this system of the LD. BIP participates in the recognition of misfolded proteins, in particular by recognizing hydrophobic regions exposed in an aqueous environment [129, 130]. The LD proteome also contains PUB39, belonging to the family of U Box proteins. U box proteins are a family of E3 ubiquitin-protein ligases [131]. E3 ligase participates in the last reaction of the ubiquitination mechanism by recognizing misfolded substrates. Four 26S proteasome proteins (Phatr3_draftJ706, Phatr3_J45122, Phatr3_EG00274, Phatr3_J11735) were also detected in the unfiltered proteome, as well as a protein involved in the recognition of misfolded proteins, a C-type lectin domain family 4 member F (CLEC4F - Phatr3_J50047) (Supplemental Table 1). Altogether, the presence of protein involved in ubiquitination processes and members of the ERAD pathway in the LD proteome suggests that control of the misfolded proteins is achieved at the periphery of this organelle.

Detection of misfolded proteins occurs downstream protein synthesis and folding. Consistently, chaperones, including four heat shock proteins (HSP, Phatr3_J46448; HSP70A, Phatr3_J54019; HSP90, Phatr3_J55230, and HSP40, Phatr3_J15138) were detected (Table 1). The translation of mRNA into proteins at the periphery of LDs is further supported by the presence of 40S and 60S ribosomal subunits and three components of RNA translation machinery, *i.e.* Elongation factors 1-alpha and 2 (EF1A, Phatr3_J28737; EF2, Phatr3_J35766) and the Eukaryotic translation initiation factor 4A (EIF4A, Phatr3_J25743). Since aminoacids are nitrogen-rich molecules, protein synthesis is not expected in a nitrogen starved context [121, 132, 133], so the presence of this equipment could find a rational, either for the translation of a specific subset of mRNA, or in preparation of a massive production of proteins when the cells

are not stressed any more. In line with this hypothesis, the RAE1 (Ribonucleic Acid Export 1) component of nuclear pore complex, involved in mRNA export [134], was not immunodetected in whole cell extracts after cultivation in the absence of nitrogen (Figure 5). We can therefore suppose that the recovery of cells relies on mRNAs stored in the cytosol during starvation. The vicinity of LDs might represent such a site for storing specific pools of mRNA.

4.6. A site for histone protein storage?

Eventually, we detected four histones (H2B-1B, Phatr3_J54360; H3-1C, Phatr3_J50872; H3.3, Phatr3_J21239 and H4-1B, Phatr3_J34971) in the purified fraction of LDs. These histones are components of the octamer forming the nucleosomes. When also considering proteins with less than 3 trypsin peptides (240 proteins, Supplemental Table 1), we could also detect other histones of the nucleosome (H2A-3A, Phatr3_J34798; H2A-1, Phatr3_J28445) as well as the H1 linker (H1, Phatr3_J44318). Histones were detected in purified fractions of LDs from other organisms: *Drosophila melanogaster* young whole embryos [135], the tobacco sphinx *Manduca sexta* [136], the filamentous fungi *Mortierella alpina* [137], Mammalian cells like adipocyte [138], macrophages [139], β-pancreatic cells [140] and in adipose tissue [141].

In the case of *Drosophila melanogaster*, whereas present in embryo, these histones were not detected in the abdominal fatbody proteome [142]. The specific association of histones to embryo-LDs is ensured by the Jabba protein [88]. We did not identify any Jabba homologue in the genome of *P. tricornutum*, suggesting that another protein might recruit histones to the surface of LDs. The storage of these nucleosome components may prepare cell division and chromatin packaging, when cells are not stressed anymore.

4.7. Can we learn from a proteome obtained with a lower stringency?

Proteomic analyses of the LD allowed the detection of 326 proteins in the purified fraction. We applied two filters to limit the detection of unspecific contaminants, one based on peptide stringency and one based on a decrease at whole cell level following nitrogen starvation. These filters have reduced the number of proteins to 86. Although it helped remove unspecific contaminants, as stated above, this procedure may also lead to a loss of information on the protein composition of LDs. We sought whether components commonly encountered in LD proteomes, had been identified in this initial list. Concerning LD biogenesis, Seipin is an ER protein having two transmembrane domains and a luminal loop, involved in LD early development [143]. A functional study of *P. tricornutum* Seipin (Phatr3_J47296) suggests a similar role [78]. This protein is generally not detected in LD proteomes and we did not detect

this sequence in the initial list, consistently with Western blot analyses (Figure 5). Concerning TAG biosynthesis, we did not detect any enzymes responsible for the last step of synthesis, such as DGAT or PDAT, often detected in LDs. In the set of 86 proteins, three proteins were detected as participating in lipid metabolism: a fatty acid synthesis enzyme, Acetyl-CoA carboxylase 1 (ACC1, Phatr3_EG01955) and two proteins involved in acyl-CoA homeostasis, a long chain acyl-CoA synthetase 4 (ACS4, Phatr3_J45510), a class II protein, and a LD acyl-CoA binding protein (LD-ACBD, Phatr3_J48778) previously described [49]. In the unfiltered set, we could detect 11 proteins involved in lipid metabolism, including fatty acid synthesis (triose phosphate/phosphate translocator, TPT1, Phatr3_J24610; 3R-hydroxyacyl-ACP dehydrase, FABZ_1, Phatr3_J1143), acyl-CoA biosynthesis (long chain acyl-CoA synthetase, ACS1, Phatr3_J20143) and β-oxydation in the mitochondrion (acyl-CoA deshydrogenase-like protein, ACAD, Phatr3_J11014) (Supplemental Table 1). CGI-58 is one of the proteins frequently associated with LDs [79-81] (Phatr3_J54974) and past studies in the diatom *Thalassiosira pseudonana* indicated a role of CGI-58 in LD hydrolysis [144]. CGI-58 was neither detected in the unfiltered LD proteome, nor by LD immunostaining with an anti-CGI-58 antibody (Figure 5) Either CGI-58 is localized at the peroxisome level as in higher plants [145], or it might associate to LDs in conditions where TAGs need to be hydrolyzed. Eventually, the detection of TPT1 (Phatr3_J24610) in the unfiltered proteome of *P. tricornutum* LD supports a tight association with the surface of the outermost membrane of the plastid. We have developed an antibody against TPT1, with a moderate reactivity at the whole cell level (Figure 5). The lack of immunodetection of TPT1 in LD fraction therefore indicates that only a minor part of this transporter is associated to the LD.

5. Conclusion

This work allowed the most refined characterization of the architecture of the LD in a diatom, upon nitrogen starvation. The LD of *P. tricornutum* has a hydrophobic core mainly composed of TAG. We also detected brassicasterol and *β*-carotene. The hydrophobic core is surrounded by a monolayer of polar lipids composed of DGTA (DGTA 20:5-16:1 and DGTA 20:5-16:2) and PC, possibly from the ER, and SQDG from the plastid. The extremely low content in MGDG does not support a biogenesis from the innermost two membranes (the IEM and OEM) of the plastid. Together with electron microscopy observation and the detection of TPT1 in the LD proteome, these results support a biogenesis of LDs from the outermost membrane of the plastid, the EpM. The origin of SQDG in the EpM, either by a transfer from more internal membranes or by in situ synthesis needs to be determined. Likewise, the export of a specific

DGTA molecular species from other endomembranes to the EpM had never been shown or hypothesized prior to this work. This localization is consistent with the recent discovery of a TAG lipase associated to the chloroplast limiting membranes in *P. tricornutum* [146]. The LD proteome obtained in three independent biological replicates, based on detection of at least three trypsin peptides, and following subtraction of proteins downregulated by nitrogen starvation, highlights 86 proteins, including the only protein marker known for *P. tricornutum* LD (StLDP). Based on this most 'stringent' list, free of contaminants, we could identify connections with specific compartments and families of proteins, confirmed by the identification of additional components in the unfiltered complete LD proteome. LD-associated proteins suggest connections with vesicular trafficking (coatomer, clathrin), cytoskeleton, plastid and mitochondria. Unsuspected LD-associated functions include protein synthesis (ribosomes), folding (chaperones), posttranslational modifications and quality control (ubiquitination and ERAD pathway), possibly preparing translation of specific mRNAs. The detection of all histone proteins, as previously demonstrated in LDs from drosophila embryos, also suggests the storage of these nucleosome components, preparing cell division and chromatin packaging, when cells are not stressed anymore. Functional characterization and cellular localization studies should be conducted in the future to better understand the role of these proteins in *P. tricornutum*, in the course of LD formation and degradation, and in the context of nitrogen availability and other environmental stresses.

Supplemental Table S1: List of 326 proteins identified in LDs (unfiltered proteome)

Supplemental Figure S1: Gas chromatography coupled to mass spectrometry analysis of the sterol composition of highly purified lipid droplets from *P. tricornutum*.

Acknowledgements

This work was supported by a Flagship program from the CEA High Commissioner and the French National Research Agency (Oceanomics Project No. ANR-11-BTBR-0008, GlycoAlps Project No. ANR-15-IDEX-02 and ANR-10-INBS-08 ProFI).

Table 1. Proteome of the purified LD from *Phaeodactylum tricornutum.* Protein IDs were obtained from the Ensembl database, and when available, Uniprot accessions were provided. Number of trypsin peptides, sequence coverage, sequence length and the number of predicted transmembrane domains (TM) are indicated. (*) localization based on [147].

Functional classification	Protein ID	Gene Symbol	Description	Numb. of pept	Seq. cover.	MW (kDa)	Seq. length	Score	Uniprot Accession	Numb. of TM	Localization
Fatty acids synthesis	Phatr3_EG01955	ACC1	Acetyl-CoA carboxylase 1	8	4.3	228.8	2082	68.877	B7G7S4	0	Plastid
Acyl CoA pool	Phatr3_J45510	ACS4	Long chain acyl-CoA synthetase 4	8	14.7	73.186	667	76.902	B7FXX6	0	Cytosol
	Phatr3_J48778	LD-ACBD	Lipid droplet acyl CoA binding protein (Yoneda et al., 2016)	3	13.7	38.326	351	72.793	B7G8C2	4	Cytosol / Lipid droplet
Glycolysis	Phatr3_J51128	GAPC2A	Glyceraldehyde-3-phosphate dehydrogenase	4	14.4	35.418	334	323.31	B7G6K6	0	Cytosol
	Phatr3_J22122	GAPC1	Glyceraldehyde-3-phosphate dehydrogenase	7	24.3	40.182	379	50.257	B7G5Q1	0	Cytosol
	Phatr3_J14792	PGK	Phosphoglycerate kinase	4	12.2	45.979	436	33.992	B7G6H0	0	Cytosol
Pentose phosphate pathway	Phatr3_EG02298	PGD	6-phosphogluconate dehydrogenase	3	2.3	125.38	1119	18.835		0	Cytosol
	Phatr3_J41856	TKL	Transketolase	4	5.2	77.135	711	48.093	B7FUU0	0	Cytosol
	Phatr3_J29260	TKL	Transketolase	3	4.8	74.096	684	26.285	B7G5R3	0	Cytosol
Oxaloacetate biosynthesis	Phatr3_J27976	PTPEPC2	phosphoenolpyruvate carboxylase	6	6.6	111.88	1009	40.083	B7G1G6	0	Mitochondria*
	Phatr3_J30519	PYC1	Precursor of pyruvate carboxylase	3	3.3	136.07	1252	24.278	B7GBG1	0	Mitochondria
Krebs Cycle	Phatr3_J26921	SCSBETA	Beta chain succinyl-coa synthetase	3	8.6	47.621	443	22.113	B7FXA2	0	Mitochondria
	Phatr3_J26290	ACO2	Aconitase hydratase 2	3	3.4	106.67	989	31.174	B7FUR4	0	Mitochondria
CO_2 concentration	Phatr3_J51305	CA	Carbonic anhydrase	9	34.4	31.064	282	323.31	B7FNU0	0	Plastid
Glutamate catabolism	Phatr3_J22357	GS	Glutamine synthase	7	11.3	79.635	716	58.012	B7G6Q6	0	Cytosol
Ornithine-Urea cycle	Phatr3_J13951	GDH	Glutamate dehydrogenase	3	8.2	49.458	450	19.966	B7G3X3	0	Cytosol
	Phatr3_J40880	AGMAT	Agmatinase	3	7.5	45.336	416	19.901	B7GCN5	0	Mitochondria
	Phatr3_J29702	UREC	Urease	3	4	94.032	878	19.026	B7G7W5	0	Cytosol
Oxydoreduction	Phatr3_J20885	GST	Glutathione S-transferase	3	11.7	34.621	307	18.389	B7G1M7	0	Mitochondria
Stramenopile Lipid droplet protein	Phatr3_J48859	StLDP	Stramenopile Lipid droplet protein (Yoneda et al., 2016)	4	12.3	48.904	456	35.866	B7G8M1	2	Lipid droplet
Unknown function, ER and plasma membrane	Phatr3_J13662	TM9SF	Nonaspanin	3	5.4	71.73	626	66.771	B7G2V6	9	Golgi / Endosome
Coatomer	Phatr3_J21929	COP1/ COPA	Coatomer subunit alpha	6	6	137.77	1254	89.602	B7G4Z7	0	TGN, ER, Lipid droplet ?
	Phatr3_J27518	COP1/ COPB2	Coatomer, WD associated region	3	4.9	105.92	962	28.833	B7FZS9	0	TGN, ER, Lipid droplet ?
Clathrin vesicle Formation	Phatr3_EG01984	CHC	Clathrin heavy chain	8	6.2	188.26	1672	121.18	B7G4Y3	0	Endocytic vesicles
	Phatr3_draftJ1735	PTAP1/2BETA	Beta subunit of clathrin adaptor complex AP2	5	6.7	98.631	890	58.116	B7S4C6	0	Plasma membrane
V-ATPase	Phatr3_J51058	VATPase	V-type H-atpase subunit	3	13.7	27.891	255	29.119	B7G360	0	Endosome
ABC transporter	Phatr3_EG02323	ABC	ABC-transporter like protein, partial	7	4.3	253.01	2256	110.97	B7G0T6	1	Plasma membrane
Inner mitochondrial envelope membrane	Phatr3_J22873	SLC25A4	Adenine nucleotide translocator; ATP/ADP translocase	4	13.5	32.703	303	36.031	B7G8Y4	2	Mitochondria
HSP proteins - stress response	Phatr3_J46448	HSP	Heat shock protein, partial	5	20.3	31.711	281	323.31	B7G195	0	Cytosol ?
	Phatr3_J54019	HSP70A	Heat shock protein HSP70 (Yoneda et al., 2016)	12	23.1	70.961	653	304	B7FQ84	0	Cytosol
	Phatr3_J55230	HSP90	Heat shock protein 90	7	11.8	80.548	709	97.087	B7GES3	0	Cytosol
	Phatr3_J15138	HSP40	Heat shock protein 40/DnaJ heat shock protein (cochaperone of HSP70)	4	8	63.687	590	56.924	B7G7Z2	2	Cytosol
Mitochondria-targeted chaperonin	Phatr3_J24820	CPN60	Chaperonin 60	3	6.6	62.509	594	25.989	B7FQ72	0	Mitochondria
Protein phosphorylation	Phatr3_EG02389	EPK2	EPK 2, cAMP-dependent protein kinase, partial	5	9.4	89.85	819	221.61	B7FUN1	0	Cytosol

	Phatr3_J45679	STK	Serine/threonine-protein kinase	3	6.2	75.453	713	54.773	B7FYI1	1	ER
Ubiquitination	Phatr3_J27118	UBI3	Ubiquitin extension protein 3	3	26.5	17.808	155	24.62	B7FY02	0	Cytosol / Nucleus ?
	Phatr3_J46098	PUB39	U-box domain-containing protein 39	4	9.4	66.442	618	53.625	B7G022	0	Unknown
Ubiquitin-dependent degradation by the proteasome	Phatr3_J1884	LAP	Leucyl aminopeptidase	5	11.1	66.881	629	48.741	B7FVX9	0	Cytosol
ER associated protein degradation (ERAD)	Phatr3_J54642	HCDC48	AAA-type ATPase Cdc48	3	5.1	88.486	800	33.986	B5Y3R0	0	Plastid
	Phatr3_EG02643	BIP	ER luminal binding protein	6	10.5	72.265	659	46.858	B7FUB7	0	Endoplasmic reticulum
Cytoskeleton	Phatr3_J51157	ACT1	Actin/actin like protein	4	10.9	41.79	377	104.05	B7G878	0	Cytoskeleton
	Phatr3_J21122	TUBB	Tubulin beta	6	16.6	49.581	447	85.959	B5Y3W7	0	Cytoskeleton
	Phatr3_J54534	TUBB	Tubulin beta	4	10.9	49.747	451	47.266	B7G0C3	0	Cytoskeleton
40S small ribosomal subunit	Phatr3_J6847	RPS9	Ribosomal protein 9	3	18.8	21.272	186	100.7	B7FXJ2	0	Cytosol
	Phatr3_J30486	RPS18	Ribosomal protein 18 40S small ribosomal subunit	5	32.6	16.488	141	155.06	B7GB86	0	Cytosol
	Phatr3_J51066	RPS19	Ribosomal protein 19 40S small ribosomal subunit	3	12.5	17.09	152	22.599	B7G3G6	0	Cytosol
	Phatr3_J17545	RPS3a	40S ribosomal protein S3a	5	19.9	28.921	261	44.111	B7FPM3	0	Cytosol
60S large ribosomal subunit	Phatr3_draftJ977	RPL4e	Ribosomal protein 4e 60S large ribosomal subunit	4	14.9	41.571	382	125.56	B7S3I7	0	Cytosol
	Phatr3_J30315	RPL18	RL18, ribosomal protein 18, 60S large ribosomal subunit	3	17.2	21.373	192	26.036	B7GAG0	0	Cytosol
	Phatr3_J30660	p0	60s acidic ribosomal protein p0	4	20.1	29.85	273	45.399	B7GBL1	0	Cytosol
Eukaryotic translation factor	Phatr3_J28737	EF1A	Elongation factor 1-alpha	4	7.1	48.055	439	76.325	B7G3C4	0	Cytosolic/ Nuclear
	Phatr3_J35766	EF2	Elongation factor 2	5	6.4	82.337	749	51.095	B7FZ72	0	Cytosolic/ Nuclear
	Phatr3_J25743	EIF4A	Eukaryotic translation initiation factor 4A	3	8.2	47.206	414	20.355	B5Y531	0	Cytosolic/ Nuclear
Ribosomes - Others	Phatr3_J54686	Era	GTPase Era	6	5.3	136.53	1226	38.352	B7G2A6	1	Mitochondria
Histone	Phatr3_J34971	H4-1B	Histone H4	5	32	11.383	103	71.208	B7FX68	0	Cytosolic/ Nuclear
	Phatr3_J21239	H3.3	Histone H3	4	22.8	15.327	136	95.474	B7G218	0	Cytosolic/ Nuclear
	Phatr3_J54360	H2B-1B	Histone H2B	3	31.9	12.629	116	115.92	B7FWR8	0	Cytosolic/ Nuclear
	Phatr3_J50872	H3-1C	Histone H3	4	25	15.312	136	13.494	B7FR39	0	Cytosolic/ Nuclear
PAP Fibrillin	Phatr3_J45813	PAPFIB	Plastid lipid-associated protein/fibrillin conserved domain protein	4	15.6	33.606	314	48.681	B7FYR9	0	Plastid
	Phatr3_J49943	PAPFIB	Plastid lipid-associated protein/fibrillin conserved domain protein	7	18.6	47.47	431	101.04	B7GCE0	0	Plastid
Pigments	Phatr3_J50705	LHCF4	Fucoxanthin-chlorophyll a-c binding protein C, chloroplastic	5	31.3	96.452	198	21.328	Q08586	0	Plastid
	Phatr3_J22006	LHCF10	Fucoxanthin chlorophyll a/c protein, chloroplastic	3	11.2	5.8	206	22.154	B7G5B6	0	Plastid
	Phatr3_J51230	LHCF11	Fucoxanthin-chlorophyll a-c binding protein F, chloroplastic	4	17.8	24.085	197	21.275	Q41094	0	Plastid
	Phatr3_J22395	LHCF8	Fucoxanthin chlorophyll a/c protein	3	13.5	11.644	200	21.651	B7G6Y1	0	Plastid
	Phatr3_J15806	PDS-LIKE3	Phytoene desaturase-like protein	3	5.6	18.915	621	68.012	B7GA36	1	Plastid
Photosynthesis	gi|118410963|ref|YP_874358.1|	psaB	Photosystem I P700 apoprotein A2	7	10.6	79.342	733	81.846	A0T0M7	10	Plastid
	gi|118410982|ref|YP_874377.1|	psbD	Photosystem II reaction center protein D2	3	9.4	78.031	351	39.077	A0T097	6	Plastid
	gi|193735613|ref|YP_874376.2|	psbC	Photosystem II chlorophyll A core antenna apoprotein CP43	3	8.7	43.852	459	50.141	A0T096	6	Plastid
	Phatr3_J4937		Rubisco expression protein	5	13.1	65.725	594	65.788	B7FR98	0	Plastid
	Phatr3_J42434		Rubisco expression protein	4	14	56.116	484	52.383	B7FR99	0	Plastid
ATP-synthase	Phatr3_J14618	ATP1	ATP synthase subunit alpha	12	26.1	58.048	544	159.28	B7G531	0	Plastid / Mitochondria ?
	Phatr3_J54086	ATPB	ATP synthase subunit beta	5	15	53.618	501	119.04	B7FS46	0	Plastid
	Phatr3_J20657	ATPC	ATP synthase gamma chain	7	26.9	42.297	390	71.62	Q41075	0	Plastid

	Phatr3_J24978	ATPCF1	ATP synthase CF1 alpha subunit	4	11.1	55.922	506	107.56	B7FQQ8	0	Plastid
	gi|118411012|ref|YP_874407.1|	atpB	ATP synthase CF1 beta chain	4	12	51.62	475	27.984	A0T0D2	0	Plastid
	gi|118411031|ref|YP_874426.1|	atpA	ATP synthase CF1 alpha chain	5	8.7	54.621	505	6.7554	A0T0F1	0	Plastid
Predicted protein	Phatr3_J44488		Predicted protein	4	6.4	55.136	530	321.14	B7FUA4	0	Signal peptide
	Phatr3_J50215		Predicted protein	6	22.6	37.645	350	134.41	B7FXS8	0	Signal peptide
	Phatr3_J49286		Predicted protein	5	19.9	31.929	301	112.6	B7GA37	0	Signal peptide
	Phatr3_EG00979		Predicted protein, partial	3	14.2	30.696	289	26.467		0	?
	Phatr3_J55010		Predicted protein	3	3.1	92.085	843	40.202	B7G9R3	0	Plastid ?
	Phatr3_J50214		Predicted protein	5	19	38.707	358	20.143	B7FXS9	0	Signal peptide
	Phatr3_J50236		Predicted protein	4	17	27.078	264	30.499	B7GDE6	0	?
	Phatr3_J13587		Predicted protein, partial	4	7.9	61.195	572	28.494		0	?
	Phatr3_J49287		Predicted protein	4	4.7	127.71	1174	23.128	B7GA38	0	Mitochondria
	Phatr3_EG02301		Predicted protein	6	5.8	131.31	1217	43.511	B7G3N9	3	Signal peptide

References

[1] D.A. Caron, P.D. Countway, A.C. Jones, D.Y. Kim, A. Schnetzer, Marine protistan diversity, Ann Rev Mar Sci, 4 (2012) 467-493.
[2] E. Marechal, Primary Endosymbiosis: Emergence of the Primary Chloroplast and the Chromatophore, Two Independent Events, Methods Mol Biol, 1829 (2018) 3-16.
[3] G.I. McFadden, Chloroplast origin and integration, Plant physiology, 125 (2001) 50-53.
[4] F.A. Wollman, An antimicrobial origin of transit peptides accounts for early endosymbiotic events, Traffic, 17 (2016) 1322-1328.
[5] D. Petroutsos, S. Amiar, H. Abida, L.-J. Dolch, O. Bastien, F. Rébeillé, J. Jouhet, D. Falconet, M.A. Block, G.I. McFadden, C. Bowler, C. Botté, E. Maréchal, Evolution of galactoglycerolipid biosynthetic pathways – From cyanobacteria to primary plastids and from primary to secondary plastids, Progress in Lipid Research, 54 (2014) 68-85.
[6] Z. Fussy, M. Obornik, Complex Endosymbioses I: From Primary to Complex Plastids, Multiple Independent Events, Methods Mol Biol, 1829 (2018) 17-35.
[7] T. Cavalier-Smith, Kingdom Chromista and its eight phyla: a new synthesis emphasising periplastid protein targeting, cytoskeletal and periplastid evolution, and ancient divergences, Protoplasma, 255 (2018) 297-357.
[8] A.S. Benoiston, F.M. Ibarbalz, L. Bittner, L. Guidi, O. Jahn, S. Dutkiewicz, C. Bowler, The evolution of diatoms and their biogeochemical functions, Philos Trans R Soc Lond B Biol Sci, 372 (2017).
[9] O. Levitan, J. Dinamarca, G. Hochman, P.G. Falkowski, Diatoms: a fossil fuel of the future, Trends Biotechnol, 32 (2014) 117-124.
[10] J. Lupette, Maréchal, Eric, Phytoplankton glycerolipids, challenging but promising prospects from biomedicine to green chemistry and biofuels, Wiley VCH, Weinheim, Germany ed.2018.
[11] M.A. Scaife, A.G. Smith, Towards developing algal synthetic biology, Biochem Soc Trans, 44 (2016) 716-722.
[12] J.K. Wang, M. Seibert, Prospects for commercial production of diatoms, Biotechnol Biofuels, 10 (2017) 16.
[13] C. Bowler, A.E. Allen, J.H. Badger, J. Grimwood, K. Jabbari, A. Kuo, U. Maheswari, C. Martens, F. Maumus, R.P. Otillar, E. Rayko, A. Salamov, K. Vandepoele, B. Beszteri, A. Gruber, M. Heijde, M. Katinka, T. Mock, K. Valentin, F. Verret, J.A. Berges, C. Brownlee, J.P. Cadoret, A. Chiovitti, C.J. Choi, S. Coesel, A. De Martino, J.C. Detter, C. Durkin, A. Falciatore, J. Fournet, M. Haruta, M.J. Huysman, B.D. Jenkins, K. Jiroutova, R.E. Jorgensen, Y. Joubert, A. Kaplan, N. Kroger, P.G. Kroth, J. La Roche, E. Lindquist, M. Lommer, V. Martin-Jezequel, P.J. Lopez, S. Lucas, M. Mangogna, K. McGinnis, L.K. Medlin, A. Montsant, M.P. Oudot-Le Secq, C. Napoli, M. Obornik, M.S. Parker, J.L. Petit, B.M. Porcel, N. Poulsen, M. Robison, L. Rychlewski, T.A. Rynearson, J. Schmutz, H. Shapiro, M. Siaut, M. Stanley, M.R. Sussman, A.R. Taylor, A. Vardi, P. von Dassow, W. Vyverman, A. Willis, L.S. Wyrwicz, D.S. Rokhsar, J. Weissenbach, E.V. Armbrust, B.R. Green, Y. Van de Peer, I.V. Grigoriev, The Phaeodactylum genome reveals the evolutionary history of diatom genomes, Nature, 456 (2008) 239-244.
[14] H. Abida, L.J. Dolch, C. Mei, V. Villanova, M. Conte, M.A. Block, G. Finazzi, O. Bastien, L. Tirichine, C. Bowler, F. Rebeille, D. Petroutsos, J. Jouhet, E. Marechal, Membrane glycerolipid remodeling triggered by nitrogen and phosphorus starvation in Phaeodactylum tricornutum, Plant physiology, 167 (2015) 118-136.
[15] P.G. Kroth, A.M. Bones, F. Daboussi, M.I. Ferrante, M. Jaubert, M. Kolot, M. Nymark, C. Rio Bartulos, A. Ritter, M.T. Russo, M. Serif, P. Winge, A. Falciatore, Genome editing in diatoms: achievements and goals, Plant Cell Rep, (2018).
[16] H.M. Nguyen, M. Baudet, S. Cuiné, J.-M. Adriano, D. Barthe, E. Billon, C. Bruley, F. Beisson, G. Peltier, M. Ferro, Y. Li-Beisson, Proteomic profiling of oil bodies isolated from the unicellular green

microalga Chlamydomonas reinhardtii: With focus on proteins involved in lipid metabolism, PROTEOMICS, 11 (2011) 4266-4273.
[17] J. Popko, C. Herrfurth, K. Feussner, T. Ischebeck, T. Iven, R. Haslam, M. Hamilton, O. Sayanova, J. Napier, I. Khozin-Goldberg, I. Feussner, Metabolome Analysis Reveals Betaine Lipids as Major Source for Triglyceride Formation, and the Accumulation of Sedoheptulose during Nitrogen-Starvation of Phaeodactylum tricornutum, PLoS One, 11 (2016) e0164673.
[18] S. Yao, A. Brandt, H. Egsgaard, C. Gjermansen, Neutral lipid accumulation at elevated temperature in conditional mutants of two microalgae species, Plant Physiol Biochem, 61 (2012) 71-79.
[19] A. Alboresi, G. Perin, N. Vitulo, G. Diretto, M. Block, J. Jouhet, A. Meneghesso, G. Valle, G. Giuliano, E. Marechal, T. Morosinotto, Light Remodels Lipid Biosynthesis in Nannochloropsis gaditana by Modulating Carbon Partitioning between Organelles, Plant physiology, 171 (2016) 2468-2482.
[20] L.-J. Dolch, J. Lupette, G. Tourcier, M. Bedhomme, S. Collin, L. Magneschi, M. Conte, K. Seddiki, C. Richard, E. Corre, L. Fourage, F. Laeuffer, R. Richards, M. Reith, F. Rébeillé, J. Jouhet, P. McGinn, E. Maréchal, Nitric Oxide Mediates Nitrite-Sensing and Acclimation and Triggers a Remodeling of Lipids, Plant physiology, 175 (2017) 1407.
[21] A.R. Burch, A.K. Franz, Combined nitrogen limitation and hydrogen peroxide treatment enhances neutral lipid accumulation in the marine diatom Phaeodactylum tricornutum, Bioresource Technology, 219 (2016) 559-565.
[22] J.R. Collins, B.R. Edwards, H.F. Fredricks, B.A.S. Van Mooy, LOBSTAHS: An Adduct-Based Lipidomics Strategy for Discovery and Identification of Oxidative Stress Biomarkers, Analytical Chemistry, 88 (2016) 7154-7162.
[23] J. Lupette, Jaussaud, Antoine, Vigor, Claire, Oger, Camille, Galano, Jean-Marie, Réversat, Guillaume, Vercauteren, Joseph, Jouhet, Juliette, Durand, Thierry, Maréchal, Eric, Non-enzymatic synthesis of bioactive isoprostanoids in Phaeodactylum following oxidative stress, Plant physiology, 178 (2018) 1344-1357.
[24] M. Conte, J. Lupette, K. Seddiki, C. Meï, L.-J. Dolch, V. Gros, C. Barette, F. Rébeillé, J. Jouhet, E. Maréchal, Screening for Biologically Annotated Drugs That Trigger Triacylglycerol Accumulation in the Diatom Phaeodactylum, Plant physiology, 177 (2018) 532.
[25] N. Wase, P. Black, C. DiRusso, Innovations in improving lipid production: Algal chemical genetics, Prog Lipid Res, 71 (2018) 101-123.
[26] N. Wase, B. Tu, J.W. Allen, P.N. Black, C.C. DiRusso, Identification and Metabolite Profiling of Chemical Activators of Lipid Accumulation in Green Algae, Plant physiology, 174 (2017) 2146-2165.
[27] H. Kim, S. Jang, S. Kim, Y. Yamaoka, D. Hong, W.Y. Song, I. Nishida, Y. Li-Beisson, Y. Lee, The small molecule fenpropimorph rapidly converts chloroplast membrane lipids to triacylglycerols in Chlamydomonas reinhardtii, Front Microbiol, 6 (2015) 54.
[28] T.C. Walther, J. Chung, R.V. Farese, Jr., Lipid Droplet Biogenesis, Annu Rev Cell Dev Biol, 33 (2017) 491-510.
[29] C. Zhang, P. Liu, The lipid droplet: A conserved cellular organelle, Protein Cell, 8 (2017) 796-800.
[30] D.J. Murphy, The dynamic roles of intracellular lipid droplets: from archaea to mammals, Protoplasma, 249 (2012) 541-585.
[31] D.J. Murphy, The biogenesis and functions of lipid bodies in animals, plants and microorganisms, Progress in Lipid Research, 40 (2001) 325-438.
[32] A. Pol, S.P. Gross, R.G. Parton, Biogenesis of the multifunctional lipid droplet: Lipids, proteins, and sites, The Journal of Cell Biology, 204 (2014) 635-646.
[33] F. Wilfling, J.T. Haas, T.C. Walther, R.V.F. Jr, Lipid droplet biogenesis, Current Opinion in Cell Biology, 29 (2014) 39-45.
[34] W.M. Henne, M.L. Reese, J.M. Goodman, The assembly of lipid droplets and their roles in challenged cells, EMBO J, 37 (2018).
[35] M.H. den Brok, T.K. Raaijmakers, E. Collado-Camps, G.J. Adema, Lipid Droplets as Immune Modulators in Myeloid Cells, Trends Immunol, 39 (2018) 380-392.

[36] N. Kory, R.V. Farese, Jr., T.C. Walther, Targeting Fat: Mechanisms of Protein Localization to Lipid Droplets, Trends Cell Biol, 26 (2016) 535-546.
[37] K.D. Chapman, J.M. Dyer, R.T. Mullen, Biogenesis and functions of lipid droplets in plants: Thematic Review Series: Lipid Droplet Synthesis and Metabolism: from Yeast to Man, J Lipid Res, 53 (2012) 215-226.
[38] A.H.C. Huang, Plant Lipid Droplets and Their Associated Proteins: Potential for Rapid Advances, Plant physiology, 176 (2018) 1894-1918.
[39] H. Itabe, T. Yamaguchi, S. Nimura, N. Sasabe, Perilipins: a diversity of intracellular lipid droplet proteins, Lipids Health Dis, 16 (2017) 83.
[40] E.R. Moellering, C. Benning, RNA Interference Silencing of a Major Lipid Droplet Protein Affects Lipid Droplet Size in Chlamydomonas reinhardtii, Eukaryotic cell, 9 (2010) 97-106.
[41] G.O. James, C.H. Hocart, W. Hillier, H. Chen, F. Kordbacheh, G.D. Price, M.A. Djordjevic, Fatty acid profiling of Chlamydomonas reinhardtii under nitrogen deprivation, Bioresource Technology, 102 (2011) 3343-3351.
[42] I.P. Lin, P.L. Jiang, C.S. Chen, J.T. Tzen, A unique caleosin serving as the major integral protein in oil bodies isolated from Chlorella sp. cells cultured with limited nitrogen, Plant Physiol Biochem, 61 (2012) 80-87.
[43] E. Peled, S. Leu, A. Zarka, M. Weiss, U. Pick, I. Khozin-Goldberg, S. Boussiba, Isolation of a Novel Oil Globule Protein from the Green Alga Haematococcus pluvialis (Chlorophyceae), Lipids, 46 (2011) 851-861.
[44] L. Davidi, A. Katz, U. Pick, Characterization of major lipid droplet proteins from Dunaliella, Planta, 236 (2012) 19-33.
[45] A. Javee, S.B. Sulochana, S.J. Pallissery, M. Arumugam, Major Lipid Body Protein: A Conserved Structural Component of Lipid Body Accumulated during Abiotic Stress in S. quadricauda CASA-CC202, Frontiers in Energy Research, 4 (2016).
[46] H. Siegler, O. Valerius, T. Ischebeck, J. Popko, N.J. Tourasse, O. Vallon, I. Khozin-Goldberg, G.H. Braus, I. Feussner, Analysis of the lipid body proteome of the oleaginous alga Lobosphaera incisa, BMC Plant Biology, 17 (2017) 98.
[47] S. Flori, P.-H. Jouneau, G. Finazzi, E. Maréchal, D. Falconet, Ultrastructure of the Periplastidial Compartment of the Diatom Phaeodactylum tricornutum, Protist, 167 (2016) 254-267.
[48] D. Nojima, T. Yoshino, Y. Maeda, M. Tanaka, M. Nemoto, T. Tanaka, Proteomics Analysis of Oil Body-Associated Proteins in the Oleaginous Diatom, Journal of Proteome Research, 12 (2013) 5293-5301.
[49] K. Yoneda, M. Yoshida, I. Suzuki, M.M. Watanabe, Identification of a Major Lipid Droplet Protein in a Marine Diatom Phaeodactylum tricornutum, Plant and Cell Physiology, 57 (2016) 397-406.
[50] A. Vieler, S.B. Brubaker, B. Vick, C. Benning, A Lipid Droplet Protein of Nannochloropsis with Functions Partially Analogous to Plant Oleosins, Plant physiology, 158 (2012) 1562.
[51] K. Yoneda, M. Yoshida, I. Suzuki, M.M. Watanabe, Homologous expression of lipid droplet protein-enhanced neutral lipid accumulation in the marine diatom Phaeodactylum tricornutum, J Appl Phycol, (2018).
[52] A. Falciatore, M.R. d'Alcalà, P. Croot, C. Bowler, Perception of Environmental Signals by a Marine Diatom, Science, 288 (2000) 2363-2366.
[53] K.E. Cooksey, J.B. Guckert, S.A. Williams, P.R. Callis, Fluorometric determination of the neutral lipid content of microalgal cells using Nile Red, Journal of Microbiological Methods, 6 (1987) 333-345.
[54] J. Folch, M. Lees, G.H. Sloane Stanley, A simple method for the isolation and purification of total lipides from animal tissues, J Biol Chem, 226 (1957) 497-509.
[55] D. Simionato, M.A. Block, N. La Rocca, J. Jouhet, E. Marechal, G. Finazzi, T. Morosinotto, The response of Nannochloropsis gaditana to nitrogen starvation includes de novo biosynthesis of triacylglycerols, a decrease of chloroplast galactolipids, and reorganization of the photosynthetic apparatus, Eukaryotic cell, 12 (2013) 665-676.

[56] G.E. Bligh, W.J. Dyer, A rapid method of total lipid extraction and purification., Can. J. Biochem. Physiol., 37 (1959) 911-917.
[57] J. Jouhet, E. Marechal, R. Bligny, J. Joyard, M.A. Block, Transient increase of phosphatidylcholine in plant cells in response to phosphate deprivation, FEBS letters, 544 (2003) 63-68.
[58] J. Jouhet, J. Lupette, O. Clerc, L. Magneschi, M. Bedhomme, S. Collin, S. Roy, E. Maréchal, F. Rébeillé, LC-MS/MS versus TLC plus GC methods: Consistency of glycerolipid and fatty acid profiles in microalgae and higher plant cells and effect of a nitrogen starvation, PLOS ONE, 12 (2017) e0182423.
[59] B. Deme, C. Cataye, M.A. Block, E. Marechal, J. Jouhet, Contribution of galactoglycerolipids to the 3-dimensional architecture of thylakoids, FASEB journal : official publication of the Federation of American Societies for Experimental Biology, 28 (2014) 3373-3383.
[60] C.M. Buseman, P. Tamura, A.A. Sparks, E.J. Baughman, S. Maatta, J. Zhao, M.R. Roth, S.W. Esch, J. Shah, T.D. Williams, R. Welti, Wounding Stimulates the Accumulation of Glycerolipids Containing Oxophytodienoic Acid and Dinor-Oxophytodienoic Acid in Arabidopsis Leaves, Plant physiology, 142 (2006) 28.
[61] J. Cox, M. Mann, MaxQuant enables high peptide identification rates, individualized p.p.b.-range mass accuracies and proteome-wide protein quantification, Nature Biotechnology, 26 (2008) 1367.
[62] B. Schwanhäusser, D. Busse, N. Li, G. Dittmar, J. Schuchhardt, J. Wolf, W. Chen, M. Selbach, Global quantification of mammalian gene expression control, Nature, 473 (2011) 337.
[63] T.N. Petersen, S. Brunak, G. von Heijne, H. Nielsen, SignalP 4.0: discriminating signal peptides from transmembrane regions, Nat Methods, 8 (2011) 785-786.
[64] O. Emanuelsson, H. Nielsen, G. von Heijne, ChloroP, a neural network-based method for predicting chloroplast transit peptides and their cleavage sites, Protein Sci, 8 (1999) 978-984.
[65] A. Gruber, G. Rocap, P.G. Kroth, E.V. Armbrust, T. Mock, Plastid proteome prediction for diatoms and other algae with secondary plastids of the red lineage, Plant J, 81 (2015) 519-528.
[66] E.L.L. Sonnhammer, G.v. Heijne, A. Krogh, A Hidden Markov Model for Predicting Transmembrane Helices in Protein Sequences, Proceedings of the 6th International Conference on Intelligent Systems for Molecular Biology, AAAI Press, 1998, pp. 175-182.
[67] L.P. Kozlowski, IPC – Isoelectric Point Calculator, Biology Direct, 11 (2016) 55.
[68] W.J. Hurkman, C.K. Tanaka, Solubilization of Plant Membrane Proteins for Analysis by Two-Dimensional Gel Electrophoresis, Plant physiology, 81 (1986) 802.
[69] S. Flori, P.H. Jouneau, B. Gallet, L.F. Estrozi, C. Moriscot, G. Schoehn, G. Finazzi, D. Falconet, Imaging Plastids in 2D and 3D: Confocal and Electron Microscopy, Methods Mol Biol, 1829 (2018) 113-122.
[70] D.L. Brasaemle, T. Barber, N.E. Wolins, G. Serrero, E.J. Blanchette-Mackie, C. Londos, Adipose differentiation-related protein is an ubiquitously expressed lipid storage droplet-associated protein, J Lipid Res, 38 (1997) 2249-2263.
[71] D.L. Brasaemle, N.E. Wolins, Isolation of Lipid Droplets from Cells by Density Gradient Centrifugation, Curr Protoc Cell Biol, 72 (2016) 3 15 11-13 15 13.
[72] S.W. Rampen, B.A. Abbas, S. Schouten, J.S.S. Damste, A comprehensive study of sterols in marine diatoms (Bacillariophyta): Implications for their use as tracers for diatom productivity, Limnol Oceanogr, 55 (2010) 91-105.
[73] M. Fabris, M. Matthijs, S. Carbonelle, T. Moses, J. Pollier, R. Dasseville, G.J. Baart, W. Vyverman, A. Goossens, Tracking the sterol biosynthesis pathway of the diatom Phaeodactylum tricornutum, New Phytol, 204 (2014) 521-535.
[74] S. Lopez, B. Bermudez, S. Montserrat-de la Paz, S. Jaramillo, L.M. Varela, A. Ortega-Gomez, R. Abia, F.J. Muriana, Membrane composition and dynamics: a target of bioactive virgin olive oil constituents, Biochim Biophys Acta, 1838 (2014) 1638-1656.
[75] K. Tauchi-Sato, S. Ozeki, T. Houjou, R. Taguchi, T. Fujimoto, The surface of lipid droplets is a phospholipid monolayer with a unique Fatty Acid composition, J Biol Chem, 277 (2002) 44507-44512.

[76] G. Onal, O. Kutlu, D. Gozuacik, S. Dokmeci Emre, Lipid Droplets in Health and Disease, Lipids Health Dis, 16 (2017) 128.
[77] Z. Yi, M. Xu, M. Magnusdottir, Y. Zhang, S. Brynjolfsson, W. Fu, Photo-Oxidative Stress-Driven Mutagenesis and Adaptive Evolution on the Marine Diatom Phaeodactylum tricornutum for Enhanced Carotenoid Accumulation, Marine Drugs, 13 (2015) 6138-6151.
[78] Y. Lu, X. Wang, S. Balamurugan, W.D. Yang, J.S. Liu, H.P. Dong, H.Y. Li, Identification of a putative seipin ortholog involved in lipid accumulation in marine microalga Phaeodactylum tricornutum, J Appl Phycol, 29 (2017) 2821-2829.
[79] K.L. Farquharson, Deciphering the role of CGI-58 in lipid metabolism in Arabidopsis, Plant Cell, 25 (2013) 1485.
[80] S. Park, S.K. Gidda, C.N. James, P.J. Horn, N. Khuu, D.C. Seay, J. Keereetaweep, K.D. Chapman, R.T. Mullen, J.M. Dyer, The alpha/beta hydrolase CGI-58 and peroxisomal transport protein PXA1 coregulate lipid homeostasis and signaling in Arabidopsis, Plant Cell, 25 (2013) 1726-1739.
[81] A. Khatib, Y. Arhab, A. Bentebibel, A. Abousalham, A. Noiriel, Reassessing the Potential Activities of Plant CGI-58 Protein, PLoS One, 11 (2016) e0145806.
[82] D. Moog, S.A. Rensing, J.M. Archibald, U.G. Maier, K.K. Ullrich, Localization and Evolution of Putative Triose Phosphate Translocators in the Diatom Phaeodactylum tricornutum, Genome Biol Evol, 7 (2015) 2955-2969.
[83] Y. Laizet, D. Pontier, R. Mache, M. Kuntz, Subfamily Organization and Phylogenetic Origin of Genes Encoding Plastid Lipid-Associated Proteins of the Fibrillin Type, Journal of Genome Science and Technology, 3 (2004) 19-28.
[84] A. Youssef, Y.h. Laizet, M.A. Block, E. Maréchal, J.-P. Alcaraz, T.R. Larson, D. Pontier, J. Gaffé, M. Kuntz, Plant lipid-associated fibrillin proteins condition jasmonate production under photosynthetic stress, The Plant Journal, 61 (2010) 436-445.
[85] C. Bréhélin, F. Kessler, K.J. van Wijk, Plastoglobules: versatile lipoprotein particles in plastids, Trends in Plant Science, 12 (2007) 260-266.
[86] H.D. Goold, S. Cuine, B. Legeret, Y. Liang, S. Brugiere, P. Auroy, H. Javot, M. Tardif, B. Jones, F. Beisson, G. Peltier, Y. Li-Beisson, Saturating Light Induces Sustained Accumulation of Oil in Plastidal Lipid Droplets in Chlamydomonas reinhardtii, Plant physiology, 171 (2016) 2406-2417.
[87] T. Moriyama, M. Toyoshima, M. Saito, H. Wada, N. Sato, Revisiting the Algal "Chloroplast Lipid Droplet": The Absence of an Entity That Is Unlikely to Exist, Plant physiology, 176 (2018) 1519-1530.
[88] Z. Li, K. Thiel, Peter J. Thul, M. Beller, Ronald P. Kühnlein, Michael A. Welte, Lipid Droplets Control the Maternal Histone Supply of Drosophila Embryos, Current Biology, 22 (2012) 2104-2113.
[89] D.L. Brasaemle, G. Dolios, L. Shapiro, R. Wang, Proteomic Analysis of Proteins Associated with Lipid Droplets of Basal and Lipolytically Stimulated 3T3-L1 Adipocytes, Journal of Biological Chemistry, 279 (2004) 46835-46842.
[90] A. Gelzinis, V. Butkus, E. Songaila, R. Augulis, A. Gall, C. Buchel, B. Robert, D. Abramavicius, D. Zigmantas, L. Valkunas, Mapping energy transfer channels in fucoxanthin-chlorophyll protein complex, Biochim Biophys Acta, 1847 (2015) 241-247.
[91] P. Kuczynska, M. Jemiola-Rzeminska, K. Strzalka, Photosynthetic Pigments in Diatoms, Mar Drugs, 13 (2015) 5847-5881.
[92] J.-C. Huang, F. Chen, G. Sandmann, Stress-related differential expression of multiple β-carotene ketolase genes in the unicellular green alga Haematococcus pluvialis, Journal of Biotechnology, 122 (2006) 176-185.
[93] G. Chen, B. Wang, D. Han, M. Sommerfeld, Y. Lu, F. Chen, Q. Hu, Molecular mechanisms of the coordination between astaxanthin and fatty acid biosynthesis in Haematococcus pluvialis (Chlorophyceae), The Plant Journal, 81 (2015) 95-107.
[94] K. Grünewald, J. Hirschberg, C. Hagen, Ketocarotenoid Biosynthesis Outside of Plastids in the Unicellular Green Alga Haematococcus pluvialis, Journal of Biological Chemistry, 276 (2001) 6023-6029.

[95] S. Ota, A. Morita, S. Ohnuki, A. Hirata, S. Sekida, K. Okuda, Y. Ohya, S. Kawano, Carotenoid dynamics and lipid droplet containing astaxanthin in response to light in the green alga Haematococcus pluvialis, Scientific Reports, 8 (2018) 5617.
[96] T.S. Moore, Phosphatidylcholine synthesis in castor bean endosperm, Plant physiology, 57 (1976) 382-386.
[97] T.S. Moore, Z. Du, Z. Chen, Membrane lipid biosynthesis in Chlamydomonas reinhardtii. In vitro biosynthesis of diacylglyceryltrimethylhomoserine, Plant physiology, 125 (2001) 423-429.
[98] R. Bartz, W.H. Li, B. Venables, J.K. Zehmer, M.R. Roth, R. Welti, R.G. Anderson, P. Liu, K.D. Chapman, Lipidomics reveals that adiposomes store ether lipids and mediate phospholipid traffic, J Lipid Res, 48 (2007) 837-847.
[99] K. Grillitsch, M. Connerth, H. Kofeler, T.N. Arrey, B. Rietschel, B. Wagner, M. Karas, G. Daum, Lipid particles/droplets of the yeast Saccharomyces cerevisiae revisited: lipidome meets proteome, Biochim Biophys Acta, 1811 (2011) 1165-1176.
[100] V.A. Ivashov, K. Grillitsch, H. Koefeler, E. Leitner, D. Baeumlisberger, M. Karas, G. Daum, Lipidome and proteome of lipid droplets from the methylotrophic yeast Pichia pastoris, Biochim Biophys Acta, 1831 (2013) 282-290.
[101] C. Botella, E. Sautron, L. Boudiere, M. Michaud, E. Dubots, Y. Yamaryo-Botte, C. Albrieux, E. Marechal, M.A. Block, J. Jouhet, ALA10, a Phospholipid Flippase, Controls FAD2/FAD3 Desaturation of Phosphatidylcholine in the ER and Affects Chloroplast Lipid Composition in Arabidopsis thaliana, Plant physiology, 170 (2016) 1300-1314.
[102] C.Y. Botte, Y. Yamaryo-Botte, T.W. Rupasinghe, K.A. Mullin, J.I. MacRae, T.P. Spurck, M. Kalanon, M.J. Shears, R.L. Coppel, P.K. Crellin, E. Marechal, M.J. McConville, G.I. McFadden, Atypical lipid composition in the purified relict plastid (apicoplast) of malaria parasites, Proc Natl Acad Sci U S A, 110 (2013) 7506-7511.
[103] B.A. Van Mooy, H.F. Fredricks, B.E. Pedler, S.T. Dyhrman, D.M. Karl, M. Koblizek, M.W. Lomas, T.J. Mincer, L.R. Moore, T. Moutin, M.S. Rappe, E.A. Webb, Phytoplankton in the ocean use non-phosphorus lipids in response to phosphorus scarcity, Nature, 458 (2009) 69-72.
[104] C. Benning, Z.H. Huang, D.A. Gage, Accumulation of a novel glycolipid and a betaine lipid in cells of Rhodobacter sphaeroides grown under phosphate limitation, Arch Biochem Biophys, 317 (1995) 103-111.
[105] L.J. Dolch, E. Marechal, Inventory of fatty acid desaturases in the pennate diatom Phaeodactylum tricornutum, Mar Drugs, 13 (2015) 1317-1339.
[106] O. Sayanova, J.A. Napier, Transgenic oilseed crops as an alternative to fish oils, Prostaglandins Leukot Essent Fatty Acids, 85 (2011) 253-260.
[107] O. Sayanova, V. Mimouni, L. Ulmann, A. Morant-Manceau, V. Pasquet, B. Schoefs, J.A. Napier, Modulation of lipid biosynthesis by stress in diatoms, Philos Trans R Soc Lond B Biol Sci, 372 (2017).
[108] W.R. Riekhof, B.B. Sears, C. Benning, Annotation of genes involved in glycerolipid biosynthesis in Chlamydomonas reinhardtii: discovery of the betaine lipid synthase BTA1Cr, Eukaryotic cell, 4 (2005) 242-252.
[109] H. Murakami, T. Nobusawa, K. Hori, M. Shimojima, H. Ohta, Betaine Lipid Is Crucial for Adapting to Low Temperature and Phosphate Deficiency in Nannochloropsis, Plant physiology, 177 (2018) 181-193.
[110] L. Alipanah, J. Rohloff, P. Winge, A.M. Bones, T. Brembu, Whole-cell response to nitrogen deprivation in the diatom Phaeodactylum tricornutum, J Exp Bot, 66 (2015) 6281-6296.
[111] O. Levitan, J. Dinamarca, E. Zelzion, D.S. Lun, L.T. Guerra, M.K. Kim, J. Kim, B.A. Van Mooy, D. Bhattacharya, P.G. Falkowski, Remodeling of intermediate metabolism in the diatom Phaeodactylum tricornutum under nitrogen stress, Proc Natl Acad Sci U S A, 112 (2015) 412-417.
[112] R. Beck, M. Rawet, F.T. Wieland, D. Cassel, The COPI system: molecular mechanisms and function, FEBS letters, 583 (2009) 2701-2709.

[113] M. Beller, C. Sztalryd, N. Southall, M. Bell, H. Jackle, D.S. Auld, B. Oliver, COPI complex is a regulator of lipid homeostasis, PLoS Biol, 6 (2008) e292.
[114] W. Wang, S. Wei, L. Li, X. Su, C. Du, F. Li, B. Geng, P. Liu, G. Xu, Proteomic analysis of murine testes lipid droplets, Sci Rep, 5 (2015) 12070.
[115] T. Serafini, L. Orci, M. Amherdt, M. Brunner, R.A. Kahn, J.E. Rothman, ADP-ribosylation factor is a subunit of the coat of Golgi-derived COP-coated vesicles: a novel role for a GTP-binding protein, Cell, 67 (1991) 239-253.
[116] F. Wilfling, A.R. Thiam, M.J. Olarte, J. Wang, R. Beck, T.J. Gould, E.S. Allgeyer, F. Pincet, J. Bewersdorf, R.V. Farese, Jr., T.C. Walther, Arf1/COPI machinery acts directly on lipid droplets and enables their connection to the ER for protein targeting, Elife, 3 (2014) e01607.
[117] G. Jurgens, Membrane trafficking in plants, Annu Rev Cell Dev Biol, 20 (2004) 481-504.
[118] Y. Guo, C. Chang, R. Huang, B. Liu, L. Bao, W. Liu, AP1 is essential for generation of autophagosomes from the trans-Golgi network, J Cell Sci, 125 (2012) 1706-1715.
[119] K. Soreng, T.P. Neufeld, A. Simonsen, Membrane Trafficking in Autophagy, Int Rev Cell Mol Biol, 336 (2018) 1-92.
[120] S. Martens, H.T. McMahon, Mechanisms of membrane fusion: disparate players and common principles, Nat Rev Mol Cell Biol, 9 (2008) 543-556.
[121] J. Longworth, D. Wu, M. Huete-Ortega, P.C. Wright, S. Vaidyanathan, Proteome response of Phaeodactylum tricornutum, during lipid accumulation induced by nitrogen depletion, Algal Res, 18 (2016) 213-224.
[122] T. Ma, Y.Y. Li, J. Zhu, L.L. Fan, W.D. Du, C.H. Wu, G.P. Sun, J.B. Li, Enhanced autophagic flux by endoplasmic reticulum stress in human hepatocellular carcinoma cells contributes to the maintenance of cell viability, Oncol Rep, 30 (2013) 433-440.
[123] B. Pajak, M. Songin, J.B. Strosznajder, A. Orzechowski, B. Gajkowska, Ultrastructural evidence of amyloid beta-induced autophagy in PC12 cells, Folia Neuropathol, 47 (2009) 252-258.
[124] N. Nelson, N. Perzov, A. Cohen, K. Hagai, V. Padler, H. Nelson, The cellular biology of proton-motive force generation by V-ATPases, J Exp Biol, 203 (2000) 89-95.
[125] Q. Shi, H. Araie, R.K. Bakku, Y. Fukao, R. Rakwal, I. Suzuki, Y. Shiraiwa, Proteomic analysis of lipid body from the alkenone-producing marine haptophyte alga Tisochrysis lutea, Proteomics, 15 (2015) 4145-4158.
[126] S. D'Andrea, Lipid droplet mobilization: The different ways to loosen the purse strings, Biochimie, 120 (2016) 17-27.
[127] C. Deruyffelaere, Z. Purkrtova, I. Bouchez, B. Collet, J.L. Cacas, T. Chardot, J.L. Gallois, S. D'Andrea, PUX10 associates with CDC48A and regulates the dislocation of ubiquitinated oleosins from seed lipid droplets, Plant Cell, (2018).
[128] F.K. Kretzschmar, L.F. Mengel, A. Muller, K. Schmitt, K.F. Blersch, O. Valerius, G. Braus, T. Ischebeck, PUX10 is a lipid droplet-localized scaffold protein that interacts with CDC48 and is involved in the degradation of lipid droplet proteins, Plant Cell, (2018).
[129] Y. Okuda-Shimizu, L.M. Hendershot, Characterization of an ERAD pathway for nonglycosylated BiP substrates, which require Herp, Mol Cell, 28 (2007) 544-554.
[130] J. Stevenson, E.Y. Huang, J.A. Olzmann, Endoplasmic Reticulum-Associated Degradation and Lipid Homeostasis, Annu Rev Nutr, 36 (2016) 511-542.
[131] S. Hatakeyama, M. Yada, M. Matsumoto, N. Ishida, K.-I. Nakayama, U Box Proteins as a New Family of Ubiquitin-Protein Ligases, Journal of Biological Chemistry, 276 (2001) 33111-33120.
[132] S. Schmollinger, T. Muhlhaus, N.R. Boyle, I.K. Blaby, D. Casero, T. Mettler, J.L. Moseley, J. Kropat, F. Sommer, D. Strenkert, D. Hemme, M. Pellegrini, A.R. Grossman, M. Stitt, M. Schroda, S.S. Merchant, Nitrogen-Sparing Mechanisms in Chlamydomonas Affect the Transcriptome, the Proteome, and Photosynthetic Metabolism, Plant Cell, 26 (2014) 1410-1435.

[133] J.J. Park, H. Wang, M. Gargouri, R.R. Deshpande, J.N. Skepper, F.O. Holguin, M.T. Juergens, Y. Shachar-Hill, L.M. Hicks, D.R. Gang, The response of Chlamydomonas reinhardtii to nitrogen deprivation: a systems biology analysis, Plant J, 81 (2015) 611-624.
[134] R. Satoh, K. Hagihara, R. Sugiura, Rae1-mediated nuclear export of Rnc1 is an important determinant in controlling MAPK signaling, Curr Genet, 64 (2018) 103-108.
[135] S. Cermelli, Y. Guo, S.P. Gross, M.A. Welte, The lipid-droplet proteome reveals that droplets are a protein-storage depot, Curr Biol, 16 (2006) 1783-1795.
[136] J.L. Soulages, S.J. Firdaus, S. Hartson, X. Chen, A.D. Howard, E.L. Arrese, Developmental changes in the protein composition of Manduca sexta lipid droplets, Insect Biochem Mol Biol, 42 (2012) 305-320.
[137] Y. Yu, T. Li, N. Wu, L. Jiang, X. Ji, H. Huang, The Role of Lipid Droplets in Mortierella alpina Aging Revealed by Integrative Subcellular and Whole-Cell Proteome Analysis, Scientific Reports, 7 (2017) 43896.
[138] Y. Ding, Y. Wu, R. Zeng, K. Liao, Proteomic profiling of lipid droplet-associated proteins in primary adipocytes of normal and obese mouse, Acta Biochimica et Biophysica Sinica, 44 (2012) 394-406.
[139] H.-C. Wan, R.C.N. Melo, Z. Jin, A.M. Dvorak, P.F. Weller, Roles and origins of leukocyte lipid bodies: proteomic and ultrastructural studies, The FASEB journal : official publication of the Federation of American Societies for Experimental Biology, 21 (2007) 167-178.
[140] S. Larsson, S. Resjö, M.F. Gomez, P. James, C. Holm, Characterization of the Lipid Droplet Proteome of a Clonal Insulin-producing β-Cell Line (INS-1 832/13), Journal of Proteome Research, 11 (2012) 1264-1273.
[141] X. Yu, L. Ye, H. Zhang, J. Zhao, G. Wang, C. Guo, W. Shang, Ginsenoside Rb1 ameliorates liver fat accumulation by upregulating perilipin expression in adipose tissue of db/db obese mice, Journal of Ginseng Research, 39 (2015) 199-205.
[142] M. Beller, D. Riedel, L. Jänsch, G. Dieterich, J. Wehland, H. Jäckle, R.P. Kühnlein, Characterization of the Drosophila Lipid Droplet Subproteome, Molecular & Cellular Proteomics, 5 (2006) 1082-1094.
[143] C. Lundin, R. Nordstrom, K. Wagner, C. Windpassinger, H. Andersson, G. von Heijne, I. Nilsson, Membrane topology of the human seipin protein, FEBS letters, 580 (2006) 2281-2284.
[144] E.M. Trentacoste, R.P. Shrestha, S.R. Smith, C. Gle, A.C. Hartmann, M. Hildebrand, W.H. Gerwick, Metabolic engineering of lipid catabolism increases microalgal lipid accumulation without compromising growth, Proc Natl Acad Sci U S A, 110 (2013) 19748-19753.
[145] M. Pyc, Y. Cai, M.S. Greer, O. Yurchenko, K.D. Chapman, J.M. Dyer, R.T. Mullen, Turning Over a New Leaf in Lipid Droplet Biology, Trends Plant Sci, 22 (2017) 596-609.
[146] X.L. Li, Y.F. Pan, H.H. Hu, Identification of the triacylglycerol lipase in the chloroplast envelope of the diatom Phaeodactylum tricornutum, Algal Research-Biomass Biofuels and Bioproducts, 33 (2018) 440-447.
[147] D. Ewe, M. Tachibana, S. Kikutani, A. Gruber, C. Rio Bartulos, G. Konert, A. Kaplan, Y. Matsuda, P.G. Kroth, The intracellular distribution of inorganic carbon fixing enzymes does not support the presence of a C4 pathway in the diatom Phaeodactylum tricornutum, Photosynth Res, 137 (2018) 263-280.